Metal fluxes during magmatic degassing in the oceanic crust: sulphide mineralisation at ODP site 786B, Izu Bonin forearc

Patten C.G.C.*[1], Markdahl K.[2], Pitcairn I.K.[2], Alt J.C.[3], Zack T.[4], Lahaye, Y.[5], Teagle D.A.H.[6]

*Corresponding author: clifford.patten@kit.edu

[1]Institute for Applied Geosciences Geochemistry, Karlsruhe Institute of Technology, Karlsruhe, Germany

[2]Department of Geological Sciences, Stockholm University, Stockholm, Sweden

[3]Department of Geological Sciences, University of Michigan, United States of America

[4]Department of Earth Sciences, University of Gothenburg, Sweden

[5]Geological Survey of Finland, 02150 Espoo, Finland

[6]Ocean and Earth Science, National Oceanography Centre Southampton, University of Southampton, Southampton, United Kingdom

Abstract

Volcanogenic massive sulphide deposits are enriched in metals that are either derived from the hydrothermal alteration of the basement rocks or supplied by exsolution of metal-rich volatiles during magmatic differentiation. The extent to which each process contributes to metal enrichment in these deposits varies between different tectonic settings. Ocean Drilling Program Hole 786B recovered >800 m of upper oceanic crust from a supra-subduction zone setting and includes a 30 m-thick mineralised zone. In-situ S isotopic compositions of pyrite decrease from 5.89±2.87 ‰ $\delta^{34}S$ in the upper mineralised zone down to -3.34±2.09

‰ $\delta^{34}S$ in the extensively altered central mineralisation zone, potentially indicating strong magmatic fluid input in this area. Whole rock data and in-situ trace element analyses in sulphide minerals show enrichment of Ag, As, Au, Bi, Mo, S, Se, Sb and Te in the mineralised zone. Evaluation of metal behaviour during magmatic differentiation and primary metal fertility of basement rocks suggests that degassing melt is the main source for the high Au, Se and S enrichment observed in the mineralised zone. Magmatic volatile exsolution occurred late during the magmatic differentiation (~2 wt.% MgO), concomitant with oxide crystallisation and metal depletion in the melt. Comparison of Ocean Drilling Program Hole 786B with volcanogenic massive sulphide deposits hosted by boninitic volcanic successions, such as in the Semail ophiolite, the Newfoundland Appalachians and the Flin Flon Belt, suggests that magmatic fluid exsolution could be a common mechanism for Au enrichment in bi-modal mafic volcanogenic massive sulphide deposits.

Introduction

The metals enriched in volcanogenic massive sulphide (VMS) deposits, hydrothermal ore deposits forming in extensional tectonic settings on the seafloor, are commonly considered to be derived from either hydrothermal alteration zones in the basement rocks (i.e. the lower sheeted dyke complex, Alt 1995a; Alt et al. 2010; Jowitt et al. 2012; Patten et al. 2016a) or be supplied by the exsolution of magmatic volatiles (Moss et al. 2001; Yang and Scott 2002; Sun et al. 2004; deRonde et al. 2005; Sun et al. 2015). The metal inventories of VMS deposits can be extensive with enrichments of precious (Ag, Au) and semi-metals (As, Bi, Cd, Sb, Se, Te, Tl) occurring alongside high concentrations of base metals (Cu, Pb, Zn; Hannington et al. 1991; Wohlgemuth-Ueberwasser et al. 2015; Monecke et al. 2016). It has been suggested that these enrichments of precious and semi-metals in VMS deposits are indicators of significant inputs of magmatic volatiles into the hydrothermal system (e.g. Sillitoe et al. 1996; Moss et al. 2001; Yang and Scott 2002). However, this suite of precious and semi-metals is also mobilised by hydrothermal alteration reactions in the lower sheeted dyke complex of the oceanic crust (Nesbitt et al. 1987; Patten et al. 2016a). Better

knowledge of the trace element signatures of magmatic volatile inputs would aid understanding the causes for the variable metal budgets in VMS deposits.

Ocean Drilling Program (ODP) Hole 786B in the Izu-Bonin forearc is one of the only deep holes drilled into supra-subduction oceanic crust, and recovered over 725 m of rocks from the volcanic section and the uppermost sheeted dykes (Arculus et al. 1992). A 5 m-thick, mineralised zone at 815-820 metres below seafloor (mbsf) near the bottom of the hole contains conspicuous pyrite, chlorite and sericite alteration, which based on negative $\delta^{34}S$ values (-2 to -5.5 ‰) has been interpreted to have been formed by hydrothermal fluids rich in magmatic volatiles (Alt et al. 1998).

In this study, we investigate the distributions and behaviours of trace metals in the mineralized zone of Hole 786B. We use low detection limit analytical methods for the measurement of Au and trace metal concentrations in the ODP Hole 786B drill core samples (Pitcairn et al. 2006a, b) together with in-situ trace element and S-isotope analyses by laser ablation-multicollector-inductively coupled plasma-mass spectrometry (LA-MC-ICP-MS). The objectives of this study are to characterise the mineralisation and trace metal enrichments in the mineralised zone and determine the signature of the magmatic volatile input in the hydrothermal system at ODP Hole 786B.

Geological setting

Magmatic Series

ODP Hole 786B is located in the forearc basement of the Izu Bonin Arc (Fig. 1) in oceanic crust that formed in the middle Eocene (40–45 Ma) during the initiation of subduction in the western Pacific (Mitchell et al. 1992; Cosca et al. 1998; Deschamps and Lallemand 2003). The water depth at OPD Hole 786B is 3080 m. After 103 m of sediments, Hole 786B penetrates 725 m into the volcanic section and the lava-dike transition zone of the oceanic crust. The volcanic section extends from 103 to 754 mbsf and comprises pillow lavas, volcanic breccias, lava flows and volcaniclastic sedimentary rocks (Arculus et al. 1992). The lower part of

Hole 786B, from 754 to 828 mbsf, is characterised by sheeted dykes that correspond to the transition zone between the sheeted dyke complex and the volcanic section (Arculus et al. 1992). Based on geochemistry and stratigraphic position, eight lithological units were distinguished (Arculus et al. 1992) which are grouped within four magmatic series: low Ca boninite, intermediate Ca boninite, andesite-dacite-rhyolite (ADR) and high Ca boninite (Murton et al. 1992; Pearce et al. 1992; Haraguchi and Ishii 2007). The low Ca boninite series, characterised by low Ca boninite (LCBon) and bronzite-andesite (LCBrzA), dominates the lower portion of Hole 786B below 690 mbsf and is the most primitive magmatic series (Arculus et al. 1992; Murton et al. 1992). The intermediate Ca boninite and the ADR series form the bulk of the volcanic section at Hole 786B and are interpreted to be part of the same magmatic series. The ADR series lavas are the fractionation products of the intermediate Ca boninite series. The intermediate Ca boninite series comprises intermediate Ca boninite (ICBon) and bronzite-andesite (ICBrzA; Murton et al. 1992; Pearce et al. 1992). The high Ca boninite series, comprises a few high Ca boninite (HCBon) and bronzite-andesite (HCBrzA) dykes, and records a relatively minor younger igneous episode at ca. 35 Ma associated with rifting of the proto-arc (Murton et al. 1992; Pearce et al. 1992; Mitchell et al. 1992). Differences in major and trace element compositions imply that the three boninitic series formed from different parental magmas, although the low Ti, Y and trace element concentrations of all rocks indicate a depleted mantle source metasomatised by fluids from the subducting slab (Murton et al. 1992; Pearce et al. 1992).

Alteration patterns

The alteration of the oceanic crust at Hole 786B is generally similar to that described in mid-ocean ridge (MOR) settings being dominated by low temperature (<100 °C) alteration in the volcanic section with an abrupt temperature increase (150-250 °C) corresponding roughly with the volcanic-dike transition (Alt et al. 1998). The ODP Hole 786B rocks show a higher degree of alteration (30-40 %) than MOR settings, most likely due the presence of abundant glassy material and mafic rock types (Alt et al. 1998). The volcanic section is altered to secondary smectite, Fe-oxyhydroxide, calcite and phillipsite. Breccias represent a

significant proportion of the recovered materials and show intense alteration up to 90% (Alt et al. 1998). Veins containing Fe-oxyhydroxide, celadonite, phillipsite and carbonate occur throughout the volcanic section (Alt et al. 1998). Secondary pyrite and chalcopyrite are common. Local pyrite occurs within a 7.5 m interval at 472 mbsf (Fig. 2; Alt et al. 1998). A significant increase in sulphide proportion occurs at 796 mbsf in hydrothermal altered LCBrzA delimiting the upper limit of the mineralised zone. Within the mineralised zone there are three domains that display distinct secondary mineral assemblages. The upper alteration zone (UAZ, 796-815 mbsf) is altered to secondary smectite, chlorite-smectite, chlorite, quartz, calcite, pyrite and chalcopyrite, and this alteration occurred at around 150-200 °C (Alt et al. 1998). Between 815 and 820 mbsf an intensively altered mineralised interval, referred to here as the central alteration zone (CAZ), is completely recrystallised to Mg-chlorite, quartz, sericite, pyrophyllite, albite, K-feldspar and pyrite (Alt et al. 1998). The alteration resulted from extensive mixing of seawater with hydrothermal fluids at ~250 °C (Alt et al. 1998). The secondary mineral distribution suggests that pervasive chlorite alteration by Mg-rich fluids was followed by local sericite and quartz alteration along fractures due to subsequent circulation of Mg-poor and alkali-enriched fluids (Alt et al. 1998). Below the central alteration zone down to bottom of the Hole (820-827 mbsf) is the lower alteration zone (LAZ) characterised by secondary alteration to chlorite-smectite, chlorite, quartz, albite, K-feldspar and disseminated sulphides (Alt et al. 1998).

Sampling and analytical methods

Nineteen least-altered samples from the volcanic section and 10 samples from the mineralised zone were selected for whole-rock analyses. Gold analyses were carried out at Stockholm University using a Thermo XSeries 2 inductively coupled plasma-mass spectrometer (ICP-MS) following the ultra-low detection limit method described in Pitcairn et al. (2006a) and digesting 3 g of sample. The 3σ method detection limit calculated from blank digests is 0.027 ppb. Analytical accuracy and precision were controlled through multiple analyses of CANMET reference material TDB-1 and USGS reference materials WMS-1 and CH-

4. Arsenic, Sb and Se concentrations were determined by hydride generation atomic fluorescence spectrometry (HG-AFS), using a PSA 10.055 Millennium Excalibur instrument at Stockholm University (Pitcairn et al. 2006b). Analyses were carried out on the same acid digests as those used for Au analyses. The 3σ method detection limits for As, Sb and Se are 0.059 ppb, 0.081 ppb and 0.039 ppb respectively. Reference materials TDB-1, WMS-1 and CH-4 were used to control analytical precision and accuracy (ESM 1).

In situ trace element analyses of sulphide minerals by laser ablation-ICP-MS (LA-ICP-MS) were carried out at Gothenburg University using a NWR213 nm laser coupled to an Agilent 8800QQQ mass spectrometer. Spot sizes of 20 μm were used with a laser pulse frequency of 5 Hz and a laser energy density of 4.65 $J.cm^{-2}$. Analyses of 179 points were carried out on pyrite, chalcopyrite, sphalerite, marcasite and bornite. Each analysis consisted of 22-25 s background and 20-26 s ablation. ^{34}S is used as an internal standard and sulphide phase's stoichiometric values were used for calibration. The following isotopes were monitored: ^{34}S, ^{57}Fe, ^{63}Cu, ^{66}Zn, ^{75}As, ^{77}Se, ^{95}Mo, ^{107}Ag, ^{111}Cd, ^{121}Sb, ^{125}Te, ^{197}Au, ^{208}Pb and ^{209}Bi. USGS reference material MASS-1, a pressed pellet (Fe–Zn–Cu–S) doped with 50–70 ppm As, Ag, Pb, Sb, Se and Te (Wilson et al. 2002; ESM 2) was used for calibration. Also, reference materials Po727 T1 SRM, a synthetic pyrrhotite doped with 40 ppm PGE and Au supplied by the Memorial University of Newfoundland, Sph-Upp, a naturally homogeneous sphalerite from the Plåtgruvan skarn deposit (Sweden), and non-matrix matched NIST SRM 610 and GSE-1G glasses were used as monitors to check for accuracy and precision (ESM 2). An accuracy of ~20% for sulphide LA-ICP-MS analyses is achieved using MASS-1 as the calibrant.

In-situ S isotope analyses on pyrite were performed using a Nu Plasma HR multicollector ICP-MS (LA-MC-ICP-MS) together with a Photon Machine Analyte G2 laser microprobe at the Geological Survey of Finland. Samples were ablated in He gas (gas flows = 0.4 and 0.1 l/min) within a HelEx ablation cell (Müller et al. 2009). During the ablation period, data were collected in static mode (^{32}S, ^{34}S) at medium resolution.

Single spot pyrite samples were ablated at a spatial resolution of 30 micrometers, using a laser energy density of 2.2 J/cm^2 at 4Hz. The total S signal obtained for pyrite was typically 1 V. Under these conditions, after a 20 s baseline, 30-50 s of ablation are needed to obtain an internal precision of $^{34}S/^{32}S \leqslant \pm 0.000005$ (1 SE). Two pyrite reference materials have been used for external bracketing (PPP-1; Gilbert et al. 2014) and quality control (in-house reference material Py1) of analyses. All sulphur isotope analyses are presented in δ notation relative to Canyon Diablo Troilite (CDT) in per mil (‰). The in-house reference materials Py1 have been previously measured by gas mass spectrometry. Compared to a bulk value of $\delta^{34}S_{CDT}$ -0.6 ± 0.6 ‰ (1 σ) for Py1 we have found an average value of -1.1 ± 0.44 ‰ (2s, n=11). Some of the difference in accuracy is related to heterogeneity in the in-house reference material.

Results

Whole-rock data

Major and trace element concentrations in Hole 786B rocks are highly variable due to the diverse range of rock types and the different alteration facies present (Arculus et al. 1992; Murton et al. 1992; Alt et al. 1998). Our suite of 19 least-altered samples from the volcanic section was selected based on mineralogical indicators and whole rock data. Low temperature seawater alteration in the volcanic section is extensive in Hole 786B leading to high concentrations of K_2O and Rb (Alt et al. 1998). Samples with relatively low K_2O and Rb concentrations (<1.2 wt.% and <20 ppm respectively; ESM 3) are assumed to have not been strongly affected by low temperature alteration. The degree of alteration is also estimated using the Ishikawa alteration index (AI; Ishikawa et al. 1976) and the chlorite-carbonate-pyrite index (CCPI, Large et al. 2001). The investigated samples have AI and CCPI values which do not suggest significant alteration and that they have most likely preserved their primary magmatic metal contents (ESM 3). One rhyolitic sample (64-2-83) from the volcanic section has high K_2O and Rb concentrations (4.5 wt.% and 41 ppm respectively) and a low AI value (16.4; ESM 3)is also assumed to record igneous metal concentrations. In general, we suggest

that these selected least-altered samples from the ICBon provide a reasonable indication of the primary Au, trace and base metal contents of the crust at Hole 786B (Table 1; Fig. 2). In contrast to the elemental concentrations observed in the least-altered rocks, samples from the mineralised zone show elevated metal concentrations associated with sulphide mineralisation (Fig. 2; Table 1).

Gold

Gold concentrations in Hole 786B range from 0.29 ppb to 66 ppb with mean and median values of 6.2 ppb and 1.2 ppb, respectively, with the difference between the mean and median being due to the high Au concentrations in the mineralised zone (Fig. 2). In the volcanic section, HCBon and ICBon have similar average Au concentrations with 0.81±0.46 ppb and 0.74±0.38 ppb, respectively (Table 1). These values are lower than boninites from other localities (e.g. 1.9±1.9 ppb, Hamlyn et al. 1985). The ICBrzA show similar Au concentrations to the boninitic samples (0.84±0.54 ppb, Table 1). The ADR series have more variability in Au content with decreasing concentrations from andesitic to rhyolitic compositions, ranging from 1.9 ppb to 0.32 ppb (Table 1). The ADR series average Au concentration (0.91±0.62 ppb) is lower than the average Au concentration of other BADR series (e.g. Mariana arc: 1.5 ppb, Terashima et al. 1994; Manus basin: 2.7±2.4 ppb, Jenner et al. 2012; Troodos ophiolite: 1.86±1.03 ppb, Patten et al. 2017). The minor variability within each magmatic series and the lack of correlation between Au and the alteration indexes (ESM 3) suggest that Au has not been significantly mobilised during low temperature seawater alteration of the least altered samples. In contrast, high Au concentrations occur in the highly altered rocks of the mineralised zone (average Au =15.8 ppb, range = 4.2 to 66 ppb; Table 2), which is significantly higher than in MOR mineralised transitional zones (e.g. ODP Hole 504B: 0.7±0.7 ppb, Nesbitt et al. 1987; IODP Hole 1256D: average Au = 2.2 ppb, range = 0.4 to 8.2 ppb, Patten et al. 2016a). Within the mineralised zone there is significant Au variation in the different alteration zones with Au concentrations being higher in the upper alteration zone (32±28 ppb) compared to the central and lower alteration zones (4.4±1.0 ppb and 4.7±0.77 ppb respectively; Table 1).

186 *Arsenic*

187 Arsenic concentrations in Hole 786B range from 16 ppb to 4200 ppb with mean and median values of 1300
188 ppb and 670 ppb, respectively. Like Au, the discrepancy between the mean and the median is due to the
189 high As enrichment in the mineralised zone (Fig. 2). Within the volcanic section, ICBon show higher As
190 concentrations than HCBon (430±330 ppb and 290±170 ppb, respectively; Table 1) but both values are
191 within the same order of magnitude of picrites from the Troodos ophiolite (320±81 ppb; Patten et al. 2017).
192 The ICBrzA show similar As concentrations to the boninitic samples (350±200 ppb; Table 1). The ADR
193 series show higher variability in As with concentrations ranging from 16 ppb to 3090 ppb (Table 1), but
194 their average concentration (820 ppb) is similar to that of Troodos ophiolite lavas (850±390 ppb, Patten et
195 al. 2017), although lower than similar rocks from the Manus basin (2450±930 ppb; Jenner et al. 2012). The
196 mineralised zone contains much higher As (3640±3040 ppb) which is lower but of the same order of
197 magnitude than As concentrations in MOR mineralised transitional zones (e.g. IODP Hole 1256D: average
198 As = 6580 ppb, range = 200 to 18200 ppb, Patten et al. 2016a). Decreasing As concentrations are observed
199 within the mineralised zone from the upper alteration zone (6040±3780 ppb) to the lower alteration zone
200 (1450±410 ppb; Table 1).

201 *Antimony*

202 Antimony concentrations in Hole 786B range from 11 ppb to 1350 ppb with mean and median values of
203 130 ppb and 77 ppb, respectively. Within the volcanic section, ICBon show higher Sb concentrations than
204 HCBon (96±12 ppb and 23±9 ppb respectively; Table 1). The latter has similar composition than picrites
205 from the Troodos ophiolite (33±3.3 ppb; Patten et al. 2017). The ICBrzA show similar Sb concentrations
206 than the HCBon but lower concentration than the ICBon (37±35 ppb, Table 1). The ADR series show
207 variability in Sb concentration ranging from 40 ppb to 264 ppb (Table 1) and its average concentration
208 (104±76 ppb Sb) is slightly higher than that of the Manus Basin and the Troodos ophiolite (87±37 ppb,

209 Jenner et al. 2012, and 78±36 ppb, Patten et al. 2017, respectively). The mineralised zone is significantly
210 enriched in Sb (mean Sb = 250 ppb, range = 60 to 1360 ppb), which is a similar range to that in MOR
211 settings (e.g. IODP Hole 1256D: average = 219 ppb, range = 34 to 590 ppb, Patten et al. 2016a). The upper
212 alteration zone shows the lowest concentrations (99±27 ppb) whereas the central alteration zone shows the
213 highest concentrations (average = 406 ppb, range = 68 to 1360 ppb), although the average is skewed by one
214 sample with a high Sb concentration (1360 ppb). The median value (101 ppb) of the central alteration zone
215 suggests similar concentration than the upper alteration zone (Table 1). The low alteration zone shows
216 slightly higher Sb concentrations with 230±160 ppb Sb (Table 1).

217 *Selenium*

218 Selenium concentrations in Hole 786B range from 0.76 ppb to 13500 ppb with mean and median values of
219 990 ppb and 8.3 ppb, respectively. Within the volcanic section, ICBon and HCBon have similar Se
220 concentrations (2.2±1.4 ppb and 3.6 ppb, 1.7-8.3 ppb respectively, Table 1) but these are significantly lower
221 contents than found in boninites from other localities (e.g. 53±55 ppb, Hamlyn et al. 1985). The ICBrzA
222 show slightly higher Se concentrations than the boninitic series (5.1±4.4 ppb, Table 1). The ADR series
223 show higher concentrations that the ICBrzA ranging from 1.6 ppb to 28 ppb (Table 1) but their average
224 concentration (11±11 ppb Se) is significantly lower than that of the BADR series from the Manus Basin and
225 the Troodos ophiolite (230±67 ppb, Jenner et al. 2012, and 119±56 ppb, Patten et al. 2017, respectively). In
226 the mineralised zone strong Se enrichments occur (26800±4000 ppb), which are higher than in those from
227 typical MOR settings (e.g. Hole 1256D: 1150±970 ppb, Patten et al. 2016a). Within the mineralised zone
228 Se concentrations are highly variable (Fig. 2), but Se is more enriched in the central (average = 5010 ppb,
229 range = 670 to 13500 ppb) and the lower (average Se = 1660 ppb, range = 340 to 2970 ppb) alteration zones
230 compared to the upper alteration zone (average Se = 851 ppb, range = 16 to 2110 ppb, Table 1).

Base metals

Copper, Zn and Pb concentrations in Hole 786B range from 1 to 304 ppm, 6 to 139 ppm and 1 to 16 ppm respectively (Arculus et al. 1990; Alt et al. 1998). Unlike Au, As, Sb and Se, there is little difference for Cu, Zn and Pb between the mean (57±38 ppm, 61±18 and 4.3±2.8 ppm respectively) and the median (55 ppm, 59 ppm and 4 ppm respectively) concentration values in Hole 786B because there is only moderate enrichment of Cu, Zn and Pb in the mineralised zone compared to the volcanic section (Fig. 2). In the volcanic section the HCBon and ICBon have similar base metal compositions (Table 1) and are similar to those of picrite from the Troodos ophiolite (56±5.4 ppm, 58±3.0 ppm and 1.1±0.78 ppm for Cu, Zn and Pb respectively; Patten et al. 2017 and references in there) but the Cu content is higher than average low-Ti basalt (20 ppm; Hamlyn et al. 1985). ICBrzA show similar base metal compositions to those of the boninitic series (Table 1). The average ADR series compositions (58±32 ppb, 62±19 ppm and 4.2±2.6 ppm for Cu, Zn and Pb respectively) are within the same order of magnitude as rocks from the Manus Basin (72±88 ppm, 83±16 ppm and 5.1 ±6.0 ppm respectively; Jenner et al. 2012) and the Troodos ophiolite (61±46 ppm, 99±74 and 1.3±0.4; Patten et al. 2017 and references in there). Relative to the volcanic section the Cu and Zn concentrations are higher in the upper alteration zone, significantly lower in the central alteration zone and similar in the lower alteration (Table 1; Fig. 2). No systematic Pb variation is observed in the mineralised zone.

Mineralised zone sulphide mineralogy

Upper Alteration Zone

The upper alteration zone (799-815 mbsf) is characterised by alteration of primary LCBon to corrensite, smectite and albite, with common veins of quartz and carbonate (Alt et al. 1998). Sulphides occur dominantly in quartz and carbonate veins although disseminated pyrite and chalcopyrite are also present in the matrix. Vein-hosted sulphides are pyrite with accessory sphalerite, marcasite, chalcopyrite and trace of

galena (Fig. 3A, B and C). Pyrite is either present on the vein margins as homogeneous aggregates (Fig. 3A and B) or is disseminated in the veins as variably sized euhedral to subhedral grains (Fig. 3C and D). The margins of some massive pyrite grains display porous textures that are also developed along fractures (Fig. 3A). In one sample (70.2.49), marcasite occurs as an overgrowth on massive and porous vein pyrite (Fig. 3A, B). Chalcopyrite occurs mostly within the veins (Fig. 3C). Sphalerite occurs in veins either as anhedral grains within the pyrite aggregates (Fig. 3B) or as subhedral grains associated with chalcopyrite within the veins (Fig. 3C). Chalcopyrite disease texture is common in sphalerite associated with chalcopyrite. Trace galena occurs as subhedral grains within pyrite or as late infill in pyrite fracture (Fig. 3A, B).

Central Alteration Zone

The central alteration zone (815-820 mbsf) shows a change in mineralogy and intensity of alteration relative to the upper alteration zone. The central alteration zone contains the greatest abundance of sulphides in Hole 786B, forming up to 10 modal percent. The sulphide assemblage is largely dominated by pyrite with rare chalcopyrite and sphalerite as inclusions in the pyrite (Fig. 4A, B). Pyrite occurs as euhedral to subhedral, 10-100 μm grains, disseminated within the host rock groundmass or within quartz veins (Fig. 4A, B).

Lower Alteration Zone

The lower alteration zone (820-829 mbsf) contains a lower proportion of sulphide than the central alteration zone and the host rock is altered to secondary mixed layer chlorite-smectite, chlorite, quartz, albite and K-feldspar with common quartz and carbonate veins. Sulphide mineralisation is dominated by pyrite that occurs as euhedral to subhedral 10-100 μm grains disseminated in the host rock groundmass or within quartz veins (Fig. 4C, D). Rare disseminated micrometric chalcopyrite grains also occur in the groundmass. Bornite grains are present as disseminated anhedral grains up to tens of microns (Fig. 4D, E). In places bornite shows alteration along grain boundaries to chalcopyrite and covellite (Fig. 4D, E). Trace covellite associated with chalcopyrite has been observed in one sample (Fig. 4F).

Trace element concentrations in sulphides from the Hole 798B Alteration Zones

Upper Alteration Zone

In-situ trace element analyses of sulphide minerals within the mineralised zone reveal significant variations in metal concentrations between the three main alteration zones and between the different sulphide phases. The trace metal content of massive pyrite from the upper alteration zone is highly variable, and are characterised by low Bi, Se and Te relative to pyrite from the central and lower alteration zones (Table 2). Porous pyrite grains have similar metal content to massive ones but show less variability (Table 2). Marcasite has similar trace metal concentration to the massive and porous pyrite except for Bi, Sb, Se and Te (Table 2). Positive trends between Ag, Au, Sb and Pb concentrations in pyrite from the upper alteration zone (ESM 4) suggest similar behaviour for these elements during sulphide precipitation. Laser ablation spectra of massive pyrite grains occasionally display Ag-As-Au-Sb-Pb spikes suggesting possible inclusions of sulfosalts. Sphalerite from the upper alteration zone has high Cu and Cd concentrations (Table 2) with elevated Cu concentrations due to the chalcopyrite disease texture. The few grains of galena that have been analysed show high concentrations of Ag, As, Cd, Sb and Se (Table 2). The whole rock data shows no Pb enrichment in the mineralised zone but enrichments may be masked by the high detection limit for Pb analytical method (Fig. 2). The high Pb concentrations of pyrite (Table 2) and presence of galena (Fig. 3A, B) suggest that Pb may be enriched in the upper alteration zone.

Central Alteration Zone

Pyrite grains in the central alteration zone show a different trace element signature from those from the upper alteration zone having higher Se, Te, Mo and Bi concentrations but lower Au, Ag and Pb content (Table 2). Disseminated pyrite grains and vein hosted pyrite show large ranges in trace metal concentrations as highlighted by the discrepancy between average and median values (Table 2). Median concentrations indicate that disseminated pyrite and vein hosted pyrite have similar trace metal enrichments although

disseminated pyrite is slightly more enriched in Cd, Sb, Te, Pb and Bi, whereas vein hosted pyrite has higher concentrations of As and Se (Table 2). The rare chalcopyrite and sphalerite grains present in the central alteration zone were too small for analysis.

Lower Alteration Zone

Disseminated pyrite from the lower alteration zone is characterised by generally lower trace metal concentrations than disseminated pyrite from the central alteration zone but still has higher Se, Te and Bi concentrations than the pyrite in the upper alteration zone (Table 2). Positive trends between Se-Te-(Bi) in pyrite from the central and lower alteration zone suggests similar behaviour during sulphide paragenesis (ESM 4). Bornite is characterised by elevated Se and Bi concentrations (290±140 ppm and 50±8.4 ppm respectively; Table 2). Chalcopyrite and covellite grains were too small to analyse.

Sulphur isotopes

In-situ S isotope analyses have been carried out on pyrite from the mineralised zone to supplement published whole rock and mineral data (Alt et al. 1998). Pyrite grains in veins from the upper alteration zone have $\delta^{34}S$ values ranging from 1.5 ‰ and 10.4 ‰ with an average of 5.9 ‰ (Fig. 5; ESM 5). These are similar to sulphide concentrate values from rhyolite and andesite at 705-800 mbsf, which range between 1.3 and 5.5 ‰ $\delta^{34}S$ (Alt et al. 1998; Fig. 5). Massive and porous pyrite grains from sample 69-4-48 (801.77 mbsf, ESM 5) show similar $\delta^{34}S$ values (5.1 ‰ and 4.8 ‰ respectively, Fig. 5), suggesting similar S source between these two textural groups. The $\delta^{34}S$ range in the upper alteration zone is similar to sulphide mineralisation in MOR settings, such as the transitional zone of OPD Hole 504B ($\delta^{34}S$ = 3.5 ‰, range = 2.9 ‰ to 5.0 ‰; Honnorez et al. 1986; Alt 1995b), TAG ($\delta^{34}S$ = 7.20 ‰; Gemmell and Sharpe, 1998 and references therein) and East Pacific Rise VMS deposits ($\delta^{34}S$ from 0 up to ~7 ‰; Shanks III, 2001 and references therein).

A strong shift in $\delta^{34}S$ values occurs between the upper and central alteration zones (Fig. 5). Disseminated pyrite from the central alteration zone has negative $\delta^{34}S$ values ranging from -8.86 to -0.59 ‰ and averaging -3.34 ‰ $\delta^{34}S$ (Fig. 5; ESM 5). These values are similar to bulk rock sulphide analyses from both the central and lower alteration zones that show distinctive negative $\delta^{34}S$ values ranging from -2.8 to -5.8 ‰ (Alt et al. 1998). This $\delta^{34}S$ signature is similar to that of VMS mineralisation in modern day seafloor in magmatic arc settings such as DESMOS ($\delta^{34}S$=-8.1 to -5.3 ‰; Gamo et al. 1997), Hine Hina ($\delta^{34}S$ = -4.9 ‰; Herzig et al. 1998), Brothers Volcano Rumble V ($\delta^{34}S$ = -5.3 ‰; deRonde et al. 2005) and Brothers Volcano Cone ($\delta^{34}S$ = -4.1 ‰, deRonde et al. 2005).

Discussion

Metal behaviour during magmatic differentiation

The mineralisation in the Transition Zone of Hole 786B is generated by the hydrothermal mobilisation of metals by a number of different fluid types (Alt et al. 1998). Irrespective of the sources and pathways of the fluids transporting metals to the mineralised zones, the primary bulk metal budget available for mobilisation in the oceanic crust is controlled by magmatic processes (Moss et al. 2001; Jowitt et al. 2012; Patten et al. 2017). Metal behaviour during the magmatic differentiation of supra-subduction zone oceanic crust is strikingly different from MOR settings (Sun et al. 2004; Jenner et al. 2010; Patten et al. 2017; Keith et al. 2018). In particular, the exsolution of magmatic fluids during differentiation of volatile-rich supra-subduction magmas can release significant quantities of fluid-mobile metals to the hydrothermal system (Moss et al. 2001; Yang and Scott 2002; Sun et al. 2004; Keith et al. 2018). The high oxygen fugacity of supra-subduction oceanic crust inhibits sulphide saturation of the magma and strongly chalcophile elements including Au, Cu and Se behave as incompatible elements during the early stages of magmatic differentiation (Sun et al. 2004; Jugo et al. 2009; Jenner et al. 2010, 2012; Patten et al. 2017; Keith et al. 2018). This process enables the build-up of strongly chalcophile elements in the melt, increasing its fertility.

345 During later stages of magmatic differentiation, the crystallisation of magnetite results in a major decrease
346 in oxygen fugacity and in the Fe content of the melt, which drives the reduction of the S in the melt from
347 sulphate to sulphide (Jenner et al. 2010). This "magnetite crisis" can trigger either the exsolution of
348 hydrosulphide complexes into magmatic fluids (Kamenetsky et al. 2001; Sun et al. 2004; Sun et al. 2015;
349 Keith et al. 2018) or sulphide saturation and magmatic sulphide segregation (Jenner et al. 2010, 2012; Park
350 et al. 2015). Both of these processes lead to the depletion of strongly chalcophile elements in the melt.

351 Metal distribution in the ICBon magmatic series coupled with magmatic modelling using the software
352 rhyolite-MELTS_v.1.1x (Gualda and Ghiorso 2015) provides insight into metal behaviour during magmatic
353 differentiation and the mechanisms leading to metal mobilisation in ODP Hole 786B (Fig. 6). The starting
354 composition for magmatic modelling was estimated as the median value of the most least-altered mafic
355 ICBon samples with MgO>10 wt.%, K_2O<0.5 wt.% and LOI <4 wt.% (ESM 6); these samples are used as
356 proxies for the primitive melt of the ICBon magmatic series. A pressure of 1.12 kBar is estimated for the
357 magmatic chamber based on the water depth of 3080 m at ODP Hole 786B and the upper part of layer 2A
358 at 3000 mbsf (Takahashi et al. 1998). Variable increments of H_2O (0.5 and 1.5 wt.%) and oxygen fugacity
359 (FMQ=0 and FMQ=1) were tested (Keith et al. 2018). Calculations are made on 25 °C increments from
360 1350 °C to 800 °C.

361 The so called "magnetite crisis" is generally characterised by a strong decrease in TiO_2 during the latest
362 stage of magmatic differentiation (MgO= 2-4 wt.%; Jenner et al. 2010). This decrease is not observed in the
363 ICBon series at Hole 786B due to their low TiO_2 content (0.16-0.40 wt.%). Variations in FeOt and V/Sc,
364 however, show a significant decrease at ~2 wt.% MgO suggesting the onset of oxide crystallisation (Fig. 6).
365 This is supported by modelling (Fig. 6; oxide crystallisation at 2.3-1.5 wt.% MgO depending on initial
366 parameters) and by the presence of common magnetite phenocrysts in the rhyolitic samples (Arculus et al.
367 1992). Modelling fractional crystallisation of a parental magma with 1.5 wt.% H_2O shows the best fit with
368 whole-rock data, which is consistent with high primary water content in boninite rocks from Bonin Islands

(2.2 wt.%; Dobson and O'Neil 1987). Further variations in FMQ have limited effects on fractionation path compared to the effect of water content (Fig. 6). Sulphur content as sulphide saturation (SCCS) is calculated using the method described in Liu et al. (2007) and the residual liquid composition from rhyolite-MELTS v.1.1.x modelling (Fig. 6). Whole-rock S data are dominantly well below the calculated SCSS until ~2 wt.% MgO where the whole rock and modelled values overlap. This implies that the melt is sulphide undersaturated during most of the magmatic differentiation. Below ~2 wt.% MgO, the decrease in the whole-rock S content may either be due to hydrosulphide complex exsolution or to sulphide saturation. The scarcity of magmatic sulphides in least-altered samples compared to sulphide saturated arc magmas (Georgatou et al. 2018), especially bornite which is expected to crystallise concomitant with magnetite (Jenner et al. 2010), suggests that sulphide saturation is most likely not the main process causes decreasing S content at < 2 wt.% MgO. Furthermore, sulphide segregation and later mobilisation through hydrothermal leaching is inconsistent with the S isotopic data from the central and lower alteration zones (Fig. 5). We suggest that the decreasing S content at below 2 wt.% MgO is caused primarily by exsolution of hydrosulphide bearing magmatic volatiles. The close timing between oxide crystallisation and magmatic volatile exsolution is supported by a decrease in whole rock LOI content at ~2 wt.% MgO (independent of LOI variations caused by low temperature alteration) and by modelling (water exsolution from the melt occurs at 1.86-1.91 wt.% MgO depending on initial parameters, Fig. 6) implying that S is mobilised from the melt by exsolving magmatic volatiles. Simultaneous sulphide saturation and magmatic fluid exsolution could lead to the formation of low density sulphide-gas compounds which can transport the sulphide mineral phases high into the hydrothermal system (Mungall et al. 2015) but no direct evidence for this process have been observed in this study. The Cu content in the melt generally increases during magmatic differentiation until ~2 wt.% MgO after which a strong decrease in Cu concentration occurs (Fig. 6). The close timing between the decrease of Cu in the melt and the exsolution of magmatic volatiles suggests Cu partitioning into the magmatic volatiles (Audétat and Pettke 2003; Frank et al. 2011). The calculated Cu content in the

393 melt during differentiation using a primary concentration of 40 ppm (ESM 7), the mineral and fluid
394 proportions from rhyolite-MELTS v.1.1.x and Cu partition coefficients from Bougault and Hekinian (1974),
395 Frank et al. (2011) and Lee et al. (2012; ESM 6), shows a similar pattern of concentration to the whole-rock
396 data which supports the loss of Cu from the melt by magmatic degassing. Data for Au and Se from the
397 volcanic section are too scarce and too scattered to allow the identification of clear magmatic trends (Fig.
398 6). However, the similar behaviour of Cu, Au and Se during magmatic differentiation based on experimental
399 (Frank et al. 2011; Mungall and Brenan 2014; Pokrovski et al. 2014) and empirical evidence (Peach et al.
400 1990; Jenner et al. 2010; Patten et al. 2013, 2017) suggests that Au and Se would be expected to behave
401 similarly to Cu. Overall the various magmatic trends suggest that metal mobilisation from the magmatic to
402 hydrothermal system occurred during the latest stage of magmatic differentiation in the ICBon series. The
403 melt may be an important source for the metals enriched in the mineralised zone.

404 Mineralisation processes in ODP Hole 786B

405 *The upper alteration zone*

406 The alteration mineralogy and the sulphide paragenesis in the Hole 786B mineralised zone are the result of
407 interactions between the host rock and three different fluids; magmatic fluid, rock-buffered hydrothermal
408 fluid and seawater-derived fluid. Each fluid is characterised by specific S isotopic signature, temperature,
409 pH, redox and metal content, and contributes variably to the metal enrichment in the mineralised zone.

410 The upper alteration zone mineralogy is similar to that observed in MOR transitional zone such as in IODP
411 Hole 1256D and ODP Hole 504B which host mineralised breccias (2.8 m and 18 m, respectively)
412 characterised by pyrite, sphalerite, chalcopyrite and trace galena and marcasite, and which have formed
413 from mixing of seawater with high temperature rock-buffered hydrothermal fluids (Honnorez et al. 1986;
414 Alt et al. 2010). The positive $\delta^{34}S$ signature of pyrite from the upper alteration zone (average $\delta^{34}S$ of
415 5.89±2.87 ‰, Fig. 5) can result from mixing between seawater-derived fluids ($\delta^{34}S$ of 21 ‰) and fluids

with lower $\delta^{34}S$. These latter fluids are most likely a mixture of magmatic S directly leached from the basement rocks (i.e. the lower sheeted dyke complex: 0-4 ‰, Alt et al. 1993), degassed magmatic H_2S (same $\delta^{34}S$ range than the lower sheeted dyke complex) and the S sourced from thermochemical sulfate reduction (TSR, -3.4 to 0.5 ‰ for 250-300 °C; ESM 5). Magmatic SO_2 is not stable in the low temperature range (150-200 °C) of the upper alteration zone (Herzig et al. 1998; ESM 5). Mixing of hydrothermal fluids (either rock-buffered or magmatic) with seawater derived fluids at ~150-200 °C promotes the enrichment of metals transported as low temperature sulphide complexes such Ag, As, Au and Pb (e.g. 100-200 °C; Huston and Large 1989; Hannington et al. 2014) potentially explaining the preferential enrichment of these metals in the upper alteration zone relative to the central and lower zones (Table 1 and 2; Fig. 7). The trace metal content of pyrite is sensitive to the conditions in which pyrite form (e.g. Maslennikov et al. 2009; Duran et al. 2015; Genna et al. 2015; Wohlgemuth-Uberwasser et al. 2015; Keith et al. 2016) and because it is the dominant sulphide phase in the three alteration zones, it provides additional insight into metal zonation. The preferential enrichments of Au, As, Ag and Pb in pyrite from the upper alteration zone relative to those from the central and lower alteration zones (Fig. 7) is similar to metal distributions observed in the upper part of MOR transitional zones and mafic VMS deposits (Herzig and Hannington 1995; ODP Hole 504B, Honnorez et al. 1986; Alt et al. 1989; IODP Hole 1256D, Teagle et al. 2006; Patten et al. 2016b; TAG, Petersen et al. 2000; Skouriotissa, Keith et al. 2016). The similarities with MOR systems, the alteration and mineralisation patterns, and the sulphide $\delta^{34}S$ values indicate that sulphide precipitation in the upper alteration zone occurred from mixing of hydrothermal fluids, most likely a mixture of rock-buffered and magmatic fluids, with seawater at moderate temperature (150-200 °C; Alt et al. 1998) and under reduced and near neutral conditions (Fig. 8).

The central and lower alteration zones

The central and lower alteration zones show marked changes in S isotopic values, trace metal content and alteration mineralogy relative to the upper alteration zone implying different mineralisation mechanisms.

Negative whole rock $\delta^{34}S$ values in the central and lower alteration zones were previously interpreted by Alt et al. (1998) as the result of magmatic SO_2 disproportionation. This is further supported by the in-situ pyrite analyses ($\delta^{34}S$ = -3.34±2.09 ‰, Fig. 5) of the central alteration zone. Degassing of magmatic SO_2, along H_2S, leads to S disproportionation into light $\delta^{34}S$ sulphide ($\delta^{34}S$< 0 ‰) and heavy $\delta^{34}S$ sulphate during mixing with seawater at temperatures below 300-400°C (Herzig et al. 1998; deRonde et al. 2005; ESM 5). Disproportionation of SO_2 produces acidic conditions which is supported by the presence of pyrophyllite and the bleached aspect of the samples in the central alteration zone (Herzig et al. 1998). Biogenic sulfate reduction (BSR) could also be responsible for the observed $\delta^{34}S$ values but the lack of textural evidence for BSR in the central and lower alteration zones and in the surrounding rocks, the moderately negative $\delta^{34}S$ values relative to BSR-related pyrite (<-10 ‰; Alt and Shanks 2011) and the temperature range (BSR occurs dominantly at <120 °C; Shanks III 2001; Alt and Shanks 2011) argue against this process. Over whole the circulation in the central and lower alteration zones of hydrothermal fluids buffered by magmatic volatiles is supported by the temperature shift (~ +50 °C; Alt et al. 1998), the S isotopic signature, the increase in acidity and oxygen fugacity implied by sericitic and pyrophyllitic alteration and bornite-covellite precipitation (Fig. 4 and 8; Hannington et al. 1999a), and the different trace element composition with higher Mo, S, Se, Te and Bi enrichment relative to the upper alteration zone (Table 1 and 2, Fig. 7). This metal association is characteristic of VMS associated with magmatic fluids (>300 °C; e.g. Hannington et al. 1999a, b, 2014; Keith et al. 2016).

Copper concentrations are surprisingly low in the Hole 786B mineralised zone, especially in the central alteration zone (Fig. 2) which is possibly due to localised zone refining (ESM 8). Copper solubility is strongly temperature dependent and Cu generally precipitates at high temperatures (~350 °C; Seewald and Seyfried 1990; Seyfried et al. 1999). The presence of disseminated bornite and rare covellite in the lower part of the mineralised zone and the loss of Cu associated with fluid exsolution during magmatic differentiation (Fig. 6) suggests that Cu precipitation could have occurred at deeper levels in the upper

sheeted dyke complex at higher temperatures, as locally observed in MOR settings (e.g. OPD Hole 504B, Alt et al. 1989; IODP Hole 1256D, Teagle et al. 2006; Alt et al. 2010) or laterally in higher temperature alteration zones within the LCaBon.

Source of the metals: magmatic vs leached

The alteration and sulphide mineralogy, trace element geochemistry and S isotope data all indicate that magmatic fluids have contributed significantly to the metal enrichment in the central and the lower alteration zones. However, rock-buffered hydrothermal fluids are also known to contain significant S and base metals (Cu, Zn, Pb), as well as Au, As, Sb and Se in MOR settings and ophiolites (Nesbitt et al. 1987; Alt 1995a; Jowitt et al. 2012; Patten et al. 2016a). The relative role of these two fluid types is not clear. Although the hydrothermally leached lower sheeted dyke complex (Alt 1995, Jowitt et al. 2012) has not been sampled by ODP Hole 786B drill core it is possible to investigate its primary metal fertility using the compositions of least-altered samples from the volcanic section as proxies and by normalising them to average MORB (Fig. 9a). Least altered samples from the volcanic section show significant enrichments of As, Sb and Pb relative to MORB (Fig. 9a), most likely due to metasomatic contamination of the mantle wedge by fluids from the subducting slab (Noll et al. 1996; Timm et al. 2012; Hattori and Guillot 2013; Patten et al. 2017). Gold is also enriched relative to MORB (0.34 ppb Au; Webber et al. 2013) because residual sulphide phases in the mantle are consumed during boninite melt generation (Hamlyn et al. 1985). Cu and Zn concentrations in Hole 786B are within the range of MORB (Fig. 9a). In contrast, S and Se (ICBon series median S = 291 ppm; Alt et al. 1998) show lower concentrations in Hole 786B compared to MORB (Fig. 6a) due to previous mobilisation during early mantle melting (Hamlyn et al. 1985). This implies that the primary crust in Hole 786B has a relatively high fertility of As, Au, Sb and Pb, a fertility for Cu and Zn similar to MORB and a low fertility for S and Se (Fig. 9a).

Comparing the primary metal fertility of the basement rocks to the metal enrichments in the mineralised zone allows evaluation of whether rock-buffered hydrothermal fluids or magmatic fluids have provided significant metals to the mineralisation in 786B (Fig. 9b). The basement rocks have high fertility in As, Sb and Pb and these elements are efficiently mobilised during hydrothermal leaching (e.g. Patten et al. 2017) so their moderate enrichments in the mineralised zone relative to the primary composition of the basement rocks (x6.6, x3.4 and x1.4, respectively; Fig. 9b) may be sourced from by rock-buffered hydrothermal fluids. Similarly, the slight Cu and Zn enrichment in the mineralised zone (x2.1 and x1.4, respectively) could also to be controlled by the same process (Fig. 9b). Gold, Se and S, however, show significantly higher enrichments than the other elements (x18, x399 and x39, respectively; Fig 9b) implying that hydrothermal leaching alone is not enough to account for their enrichment. In comparison, Au enrichment in MORB transitional zone is significantly lower (x6 in IODP Hole 1256D and 1.3x in ODP Hole 504B; Nesbitt et al. 1987; Patten et al. 2016a). The Au, Se and S enrichment in the mineralised zone, therefore, is controlled by magmatic fluid input in the hydrothermal system. Increase in Se/S in the central alteration zone (up to 0.54; ESM 3) suggests high H_2Se/H_2S in the ore forming fluids which also supports magmatic input of Se in the system (Huston et al. 1995).

Implication on VMS deposit formation and Au endowment.

Although the mineralisation at ODP Hole 786B is not directly comparable to VMS deposits on land in term of tonnage and grade, and as VMS deposits are not common in forearc settings, it provides nevertheless important insights into ore forming processes related to magmatic degassing as it has not been affected by extensive zone refining, boiling and metamorphism. The host rocks at OPD Hole 786B, being dominated by mafic rocks with minor felsic rocks, classifies the mineralisation system as bi-modal mafic (Barrie and Hannington, 1999). In the geological record, bi-modal mafic VMS deposits are often associated with boninite rocks (e.g. Barrie and Hannington, 1999; Piercey, 2010, 2011) which show similar petrochemical assemblage to those in ODP Hole 786B (ESM 9; Piercey et al. 2010).

In the Semail ophiolite, Oman, several VMS deposits (e.g. Aarja, Rakah, Al-Bishara) are hosted in boninite rocks within the Alley unit (Gilgen et al. 2014) which is interpreted to have formed in a supra-subduction setting (e.g. Alabaster et al. 1982; Godard et al. 2003; Haase et al. 2016). These deposits are characterised by different mineralogy, metal content and paragenetic sequence than their counterpart in the Geotimes unit (Alabaster and Pearce, 1985; Hannington et al. 1998; Gilgen et al. 2014). The Aarja deposit, for example, is characterised pyrite-marcasite-sphalerite-tenantite-galena-chalcopyrite-bornite assemblage and by high Zn, Pb, Ag, Au and As (Ixer et al. 1984, Alabaster and Pearce, 1985; Hannington et al. 1998). Although the Au grade of the Aarja deposit is not properly constrained, native gold inclusions in pyrite (Ixer et al. 1984) suggest and elevated gold grade (Gilgen et al. 2014). The VMS deposits hosted in the boninite Alley unit have higher Au grade (>0.8 ppm) than the other ones in the ophiolite (<0.4 ppm; Gilgen et al. 2014). The reason for this systematic Au enrichment is not constrained; leaching from the boninites with high Au-content or subseafloor boiling have been suggested (Gilgen et al. 2014). It is important to note that the mineralogical assemblages and metal enrichments do not preclude magmatic degassing as a possible mechanism for the Au enrichment in these deposits especially as several of them are spatially closely related to highly emplaced plagiogranite intrusions (Stake and Taylor, 2003).

The Rambler Camp in the Newfoundland Appalachians, Canada, is characterised by bi-modal mafic VMS deposits which are hosted in a thick rhyolite complex (Rambler Rhyolite formation; Piercey, 1997). The volcanic sequence, which is part of the Pacquet Harbour Group, shows a tectono-stratigraphic evolution from boninitic lavas and their differentiated products, to transitional arc volcanic rocks and MORB, which is interpreted to record the evolution of a primitive-arc to incipient back-arc settings (Piercey et al. 1997; Piercey, 2010; Skulski et al. 2010; Pilote and Piercey, 2018). The VMS deposits in the Rambler Camp are significantly enriched in Au, such as the Rambler Main deposit which classifies an auriferous VMS deposit with 5.1 ppm Au (Mercier-Langevin et al. 2011). The Ming deposit (21.9 Mt at 0.61 ppm Au) consists of several stacked lenticular ore bodies (Brueckner et al. 2014). The 1806 zone, one of the uppermost lenses,

534 is enriched in Au and Ag (4.31 ppm and 32.15 ppm, respectively) alongside As, Hg and Bi (Brueckner et
535 al. 2014). This specific metal enrichment has been interpreted to be syngenetic and strongly points toward
536 a magmatic fluid input (Brueckner et al. 2014) which is partly supported by the S isotopic signature of the
537 sulphide assemblage (Brueckner et al. 2015).

538 The Flin Flon belt, Mannitoba, Canada, hosts large Paleoproterozoic VMS deposits which are all associated
539 with juvenile arc tectono-stratigraphic assemblages (e.g. Flin Flon and Snow Lake; Syme et al. 1999). These
540 bi-modal assemblages are dominated by BADR series (Syme et al. 1999) but boninites are also present in
541 the Snow Lake arc assemblage and are closely related to VMS deposits (Sterne et al. 1995; Bailes and
542 Galley, 1999). The bi-modal mafic/felsic VMS deposits in the Flin Flon and Snow Lake arc assemblages
543 show significant Au enrichment with, for example, the Flin Flon and the Lalor deposits classified as Au
544 anomalous (>31 t Au) and the Photo Lake classified as auriferous (>3.41 ppm Au; Mercier-Langevin et al.
545 2011). These deposits have been affected by polyphase deformation and an amphibolite facies metamorphic
546 overprint which make their primary seafloor paragenesis difficult to reconstruct but the Au enrichment is
547 most likely syngenetic (Duff et al. 2015).

548 Compilation of the Ti, Fe, V/Sc and Cu concentration of the VMS hosting volcanics of the Lasail and Alley
549 unit of the Semail ophiolite (Alabaster et al. 1982; Gilgen et al. 2014; Haase et al. 2016), the lower sequence
550 of the Pacquet Harbour Group of the Baie Verte Peninsula (Piercey et al. 1997; Skulski et al. 2010; Pilote
551 and Piercey, 2018) and the juvenile arc sequences of the Flin Flon belt (Syme and Bailes; 1993; Sterne et
552 al. 1995; Syme, 1998) show similar trends with the magmatic differentiation observed at ODP Hole 786B.
553 The decrease in Ti, Fe and V/Sc during late magmatic differentiation suggest the onset of magnetite
554 crystallisation at 2-3 wt.% MgO in the Lasail and Alley units, 4-5.5 wt.% MgO in the lower Pacquet Harbour
555 Group and 2.5-4 wt.% MgO in the juvenile arc sequences of the Flin Flon belt (Fig. 10). In the three settings
556 Cu decrease in the melt is concomitant with the onset of magnetite crystallisation (Fig. 10) suggesting metal
557 mobilisation from the melt either by magmatic fluid degassing, sulphide segregation or sulphide-gas

558 compounds (Mungall et al. 2015). Further investigation is required to precisely determine which process is
559 controlling metal distribution in the melt and if there is a genetic link with the Au-bearing VMS deposits in
560 the volcanic sequences. Nevertheless these trends highlight the importance of investigating the metal
561 distribution in volcanic sequences hosting the VMS deposits in order to better constrain the magmatic-
562 hydrothermal contribution to VMS deposit metal endowment, especially for Au. Combining systematic
563 metal characterisation with classical petrochemical assemblages (Piercey, 2010) will enable to better
564 constrain large-scale metal-fluxes in VMS hosting volcanic sequences and would improve exploration
565 model mafic and bi-modal mafic/felsic VMS deposits.

566 **Conclusions**

567 Investigation of the sulphide mineralisation and the associated metal endowment in ODP Hole 786B
568 mineralised zone highlights that exsolution of magmatic fluid has a profound impact on the hydrothermal
569 system and on metal fluxes in arc-related oceanic crust. Analyses by low detection limit whole rock and in-
570 situ methods enable us to determine the role of magmatic fluid inputs on the budget and distribution of Ag,
571 As, Au, Bi, Mo, Pb, S, Se, Sb, Te and Zn in the oceanic crust at Hole 786B. This role is summarised in
572 Figure 11 and the main outcomes of the study are:

573 • The primary oceanic crust at ODP Hole 786B has high As, Au, Sb and Pb, similar Cu and Zn and
574 low S and Se concentrations relative to MORB. Arsenic, Sb and Pb high fertility is likely due to an
575 enriched metasomatised mantle source by subducting slab dehydration while Au high fertility is
576 likely due to melting of residual sulphides during boninitic melt generation. Low S and Se fertility
577 is likely due to a depleted mantled source during boninitic melt generation.

578 • Frequent magnetite phenocrysts in rhyolitic samples and variations in V/Sc and FeOt coupled with
579 modelling suggest that late oxide crystallisation (magnetite crisis) occurred at ~2 wt.% MgO during
580 magmatic differentiation. Variation in LOI content coupled with modelling also suggest that

magmatic fluid exsolution is concomitant with oxyde crystallisation. Depletion of S, Cu, and possibly Se and Au, in the magma is also observed at ~2 wt.% MgO. These depletions are interpreted to represent metal loss from the melt by magmatic degassing. This process can account for part of the metal endowment observed in the mineralised zone.

- The sulphide population in the mineralised zone can be divided in three hydrothermal domains. The upper alteration zone is characterised by vein hosted pyrite, sphalerite, galena, chalcopyrite and marcasite sulphide population with positive $\delta^{34}S$ values. Mineralisation occurs by mixing of seawater with reduced and near neutral hydrothermal fluids (a mixture of rock-buffered and magmatic fluids) at 150-200 °C. The central alteration zone is characterised by extensive disseminated pyrite mineralisation; other sulphide phases are scarce. The lower alteration zone is characterised by vein hosted and disseminated pyrite with trace bornite, covellite and chalcopyrite. Pyrite grains in the central and lower alteration zones have negative $\delta^{34}S$ values which imply a magmatic origin for S. Mineralisation occurs by intensive mixing of oxidised and acidic magmatic-buffered hydrothermal fluids with derived-seawater at ~250 °C.

- ODP Hole 786B mineralised zone shows distinct metal zonation with Ag, As, Au, enriched in the upper alteration zone and Bi, Mo, Sb, Sb and Te enriched in the central and lower alteration zones. The central alteration zone is significantly depleted in Cu and Zn. Changes in temperature, acidity and redox between the alteration domains, caused by change in fluid type mixture, were the driving mechanisms for metal zonation.

- The Hole 786B mineralisation shows some characteristics of Au-rich VMS deposits, and the strong enrichments of Au, Bi, Mo, S, Se and Te observed in the mineralised zone are interpreted to be of magmatic origin.

- Comparison of ODP Hole 786B with the VMS hosting mafic and bi-modal mafic volcanic sequences from the Semail ophiolite, the Newfoundland Appalachians and the Flin Flon Belt, suggests that magmatic fluid exsolution could be a common mechanism for Au enrichment in mafic and bi-modal mafic/felsic VMS deposits.

Acknowledgements

This work was funded by Stockholm University and by the Swedish Research Council (PRG 621-2007-4539). The authors would like to thank Steve Piercey, Tucker Barrie and Thomas Monecke for the thorough review of the manuscript. This research used samples provided by the ODP and IODP and the authors would like to thank the IODP Kochi Core Centre, Japan. The ODP was sponsored by the National Science Foundation and participating countries under management of Joint Oceanographic Institutions. The IODP was supported by the National Science Foundation; Japan's Ministry of Education, Culture, Sports, Science, and Technology; the European Consortium for Ocean Research Drilling; the Australia-New Zealand IODP Consortium; and the People's Republic of China Ministry of Science and Technology.

Figure captions

Figure 1. Location and simplified lithostratigraphy of ODP Hole 786B in the Izu-Bonin forearc. Modified from Arculus et al. (1992), Alt et al. (1998) and Haraguchi and Ishii (2007).

Figure 2. Depth profile of whole-rock data in Hole 786B. Gold, As, Se and Sb are from this study and S, Cu, Zn and Pb are from Arculus et al. (1992) and Alt et al. (1998). Pb analyses are close to the detection limit. HCBon = high Ca boninite; ICBon =intermediate Ca boninite; ICBrzA = intermediate Ca bronzite-andesite; LCBrzA = low Ca bronzite-andesite; Min. = mineralised LCBRzA; UAZ = upper alteration zone; CAZ = central alteration zone; LAZ = lower alteration zone.

Figure 3. Sulphide population of the upper alteration zone. A) Quartz vein with early massive pyrite (Py), galena (Gn) and chalcopyrite (Cpy). On the margin the pyrite is porous. Late stage marcasite (Mc)

precipitated on top of porous and massive pyrite. Sample 70-2-49. B) Same vein that A) with early sphalerite (Sp) within massive pyrite and late subhedral sphalerite disseminated within the vein. Sample 70-2-49. C) Early euhedral massive pyrite and late chalcopyrite and sphalerite. Sample 69-6-124. D) Vein hosted pyrite and discrete disseminated pyrite grains within the groundmass. Sample 69-4-48.

Figure 4. Sulphide population of the central and lower alteration zones. A) and B) Vein hosted pyrite (Py) in the central alteration zone forming a network. Trace sphalerite and chalcopyrite occur as inclusions in pyrite. A) Sample 71-1-91 and B) sample 71-1-15. C) Disseminated sulphides in the lower alteration zone dominated by pyrite. Sample 72-1-8. D) Disseminated euhedral pyrite and associated anhedral bornite (Bn). Late chalcopyrite (Cpy) exsolutions occurs on the rim of the bornite. Sample 72-1-8. E) Disseminated bornite with covellite and chalcopyrite exsolutions. Sample 72-1-8. F) Replaced chalcopyrite by covellite in the lower alteration zone. Sample 72-1-138.

Figure 5. Sulphur isotopic data for in-situ analyses of massive, porous and disseminated pyrite within the mineralised zone. The upper alteration zone is characterised by positive $\delta^{34}S$ values whereas the central and lower alteration zones are characterised by negative $\delta^{34}S$ values implying different S sources. Grey points are whole rock data from Alt et al. (1998).

Figure 6. Hole 786B ICBon-ICBrzA-ADR series whole rock data plotted versus MgO and rhyolite-MELTS v.1.1x modelling. Oxide crystallisation occurs at ~2.3-1.5 wt.% MgO as suggested by a sharp decrease in V/SC and FeOt. Magmatic fluid exsolution occurs concomitant with oxide crystallisation as suggested by LOI decrease at ~2 wt.% MgO. S concentration is below the SCSS suggesting that the melt is sulphide undersaturated during most of the magmatic differentiation. Decrease in S after oxide crystallisation is interpreted as S loss associated with magmatic fluid exsolution. Cu concentration increases until oxide crystallisation and magmatic fluid exsolution after which it is lost from the melt. Calculated Cu in the melt suggest mobilisation associated with magmatic degassing (see text for details). Too scarce data for Au and

Se enable to observe clear trends. Whole rock data are from Arculus et al. (1992) except for S which is from Alt et al. (1998) and Se and Au which are from this study; the data plot within the least altered box of the AI and CCPI alteration index (ESM 3) and represent primary magmatic values. ICBrzA = intermediate Ca bronzite-andesite; ICBon = intermediate Ca boninite. Ox in = oxide crystallisation in modelling; Fluid out = magmatic fluid exsolution in modelling.

Figure 7. Trace metal content of pyrite from the upper alteration zone versus pyrite from the central and lower alteration zones. UAZ = upper alteration zone; CLAZ = central and lower alteration zones.

Figure 8. Redox-pH diagram of the mineralisation at ODP Hole 786B transitional zone. The different alteration zones are plotted based on their mineralogical assemblage. Modified from Hannington et al. (1999).

Figure 9. A) Average concentrations of Hole 786B ICBrzA-ADR and ICBon series normalised average MORB values from Arevalo and MacDonough (2010) except for Au which is from Webber et al. (2013). Troodos ophiolite and Manus basin fresh glass data are from Jenner et al. (2012) and Patten et al. (2017). ICBrzA = intermediate Ca bronzite-andesite; ADR = andesite-dacite-rhyolite; ICBon = intermediate Ca boninite; BADR = basalt-andesite-dacite-rhyolite. B) Mineralised zone MORB normalised values versus volcanic section MORB normalised values. The high S, Se and Au concentrations in the volcanic section are due to magmatic fluid input in the hydrothermal system. V.S. = volcanic section, M.Z. = mineralised zone.

Figure 10. Ti, Fe, V/Sc and Cu variation during magmatic differentiation of A) the Lasail and Alley units of the Semail ophiolite, Oman (Alabaster et al. 1982; Gilgen et al. 2014; Haase et al. 2016); B) the lower sequence of the Pacquet Harbour Group of the Baie Verte Peninsula (Piercey et al. 1997; Skulski et al. 2010; Pilote and Piercey, 2018) and; C) the juvenile arc sequences of the Flin Flon belt (Syme and Bailes; 1993; Sterne et al. 1995; Syme, 1998). Despite alteration and metamorphism, preservation of primary magmatic

672 trends is observed. All three terranes show late oxide crystallisation (grey bar) at 2-3 wt.% MgO in Semail,
673 4-6 wt.% MgO in the Newfoundland Appalachians and 2.5-3 wt.% MgO in the Flin Flon belt. Concomitant
674 Cu decrease in the melt possibly imply magmatic degassing as in OPD Hole 786B.

675 Figure 11. Fluxes of metals in the oceanic crust at Hole 786B and paragenesis of the mineralisation in the
676 mineralised zone. Simplified physico-chemicals profiles in mineralised zone are shown. See text for details.

677 **References**

678 Alabaster T, Pearce JA, Malpas J (1982) The volcanic stratigraphy and petrogenesis of the Oman ophiolite
679 complex. Contrib to Mineral Petrol 81:168–183

680 Alabaster T, Pearce JA (1985) The interrelationship between magmatic and ore-forming hydrothermal
681 processes in the Oman ophiolite. Econ Geol 80:1–16

682 Alt JC (1995a) Subseafloor processes in mid-ocean ridge hydrothermal systems. Seafloor hydrothermal
683 systems. Phys Chem Biol Geol Interact 85–114

684 Alt JC (1995b) Sulfur isotopic profile through the oceanic crust: Sulfur mobility and seawater-crustal sulfur
685 exchange during hydrothermal alteration. Geology 23:585–588

686 Alt JC, Anderson TF, Bonnell L (1989) The geochemistry of sulfur in a 1.3 km section of hydrothermally
687 altered oceanic crust, DSDP Hole 504B. Geochim Cosmochim Acta 53:1011–1023

688 Alt JC, Dah T, Brewer T, Shanks WC, Halliday A (1998) Alteration and mineralization of an oceanic forearc
689 and the ophiolite-ocean crust analogy. J Geophys Res Solid Earth 103:12365–12380

690 Alt JC, Laverne C, Coggon RM, Teagle DAH, Banerjee NR, Morgan S, Smith-Duque CE, Harris M, Galli
691 L (2010) Subsurface structure of a submarine hydrothermal system in ocean crust formed at the East Pacific
692 Rise, ODP/IODP Site 1256. Geochem Geophys Geosyst 11

693 Alt JC, Shanks WC (2011) Microbial sulfate reduction and the sulfur budget for a complete section of altered
694 oceanic basalts, IODP Hole 1256D (eastern Pacific). Earth Planet Sci Lett 310:73–83

695 Arculus RJ, Pearce JA, Murton BJ, Van der Laan SR (1992) Igneous stratigraphy and major element
696 geochemistry of Holes 786A and 786B. Proc Ocean Drill Program Sci Results 25:143–169

697 Bailes AH, Galley AG (2000) Evolution of the Paleoproterozoic Snow Lake arc assemblage and
698 geodynamic setting for associated volcanic-hosted massive sulphide deposits, Flin Flon Belt, Manitoba,
699 Canada. Can J Earth Sci 36:1789–1805

700 Barrie CT, Hannington MD (1999) Classification of Volcanic-Associated Massive Sulfide Deposits Based
701 on Host-Rock Composition. In: Volcanic Associated Massive Sulfide Deposits: Processes and Examples in
702 Modern and Ancient Settings. Soc Econ Geol

703 Bougault H, Hekinian R (1974) Rift valley in the Atlantic Ocean near 36 50′ N: Petrology and
704 geochemistry of basaltic rocks. Earth Planet Sci Lett 24:249 – 261

705 Brueckner SM, Piercey SJ, Sylvester PJ, et al (2014) Evidence for syngenetic precious metal enrichment in
706 an Appalachian volcanogenic massive sulfide system: The 1806 Zone, Ming Mine, Newfoundland, Canada.
707 Econ Geol 109:1611–1642

708 Brueckner SM, Piercey SJ, Layne GD, et al (2015) Variations of sulphur isotope signatures in sulphides
709 from the metamorphosed Ming Cu (– Au) volcanogenic massive sulphide deposit, Newfoundland
710 Appalachians, Canada. Miner Depos 50:619–640

711 Cosca M, Arculus R, Pearce J, Mitchell J (1998) 40Ar/39Ar and K-Ar geochronological age constraints for
712 the inception and early evolution of the Izu-Bonin-Mariana arc system. Isl Arc 7:579–595

713 Deschamps A, Lallemand S (2003) Geodynamic setting of Izu-Bonin-Mariana boninites. Geol Soc London,
714 Spec Publ 219:163–185

715 Duff S, Hannington MD, Caté A, et al (2015) Major ore types of the Paleoproterozoic Lalor auriferous
716 volcanogenic massive sulphide deposit, Snow Lake, Manitoba. Target Geosci Initiat 4:147–170

717 Duran C, Barnes S-J, Corkery J (2015) Chalcophile and platinum-group element distribution in pyrites from
718 the sulfide-rich pods of the Lac des Iles Pd deposits, Western Ontario, Canada: Implications for post-
719 cumulus re-equilibration of the ore and the use of pyrite compositions in exploration. J Geochemical Explor
720 158:223–242

721 Frank MR, Simon AC, Pettke T, et al (2011) Gold and copper partitioning in magmatic-hydrothermal
722 systems at 800 C and 100 MPa. Geochim Cosmochim Acta 75:2470–2482

723 Gamo T, Okamura K, Charlou J-L, Urabe T, Auzende J-M, Ishibashi J, Shitashima K, Chiba H (1997)
724 Acidic and sulfate-rich hydrothermal fluids from the Manus back-arc basin, Papua New Guinea. Geol
725 25:139–142

726 Gemmell JB, Sharpe R (1998) Detailed sulfur-isotope investigation of the TAG hydrothermal mound and
727 stockwork zone, 26 N, Mid-Atlantic Ridge. Proc Ocean Drill Program Sci Res 71–84

728 Genna D, Gaboury D (2015) Deciphering the hydrothermal evolution of a VMS System by LA-ICP-MS
729 using trace elements in pyrite: an example from the Bracemac-McLeod Deposits, Abitibi, Canada, and
730 implications for exploration. Econ Geol 110:2087–2108

731 Georgatou A, Chiaradia M, Rezeau H, Wälle M (2018) Magmatic sulphides in Quaternary Ecuadorian arc
732 magmas. Lithos 296:580–599

733 Gilbert SE, Danyushevsky LV, Rodermann T, Shimizu A, Gurenko A, Meffre S, Thomas H, Large RR,
734 Death D (2014) Optimisation of laser parameters for the analysis of sulphur isotopes in sulphide minerals
735 by laser ablation ICP-MS. J Anal At Spectrom 29:1042

736 Gilgen SA, Diamond LW, Mercolli I, et al (2014) Volcanostratigraphic controls on the occurrence of
737 massive sulfide deposits in the Semail Ophiolite, Oman. Econ Geol 109:1585–1610

738 Haase KM, Freund S, Beier C, et al (2016) Constraints on the magmatic evolution of the oceanic crust from
739 plagiogranite intrusions in the Oman ophiolite. Contrib to Mineral Petrol 171:46

740 Hamlyn PR, Keays RR, Cameron WE, Crawford AJ, Waldron HM (1985) Precious metals in magnesian
741 low-Ti lavas: Implications for metallogenesis and sulfur saturation in primary magmas. Geochim
742 Cosmochim Acta 49:1797–1811

743 Hannington M, Herzig P, Scott S, et al (1991) Comparative mineralogy and geochemistry of gold-bearing
744 sulfide deposits on the mid-ocean ridges. Mar Geol 101:217–248

745 Hannington MD, Galley AG, Herzig PM, Petersen S (1998) Comparison of the TAG mound and stockwork
746 complex with Cyprus-type massive sulfide deposits. Proc Ocean Drill Program Sci Res 158: 389-415

747 Hannington MD, Poulsen KH, Thompson JFH, Sillitoe RH (1999a) Volcanogenic gold in the massive
748 sulfide environment Volcanic-associated massive sulfide deposits: Processes and examples in modern and
749 ancient settings. Rev Econ Geol 8:325–356

750 Haraguchi S, Ishii T (2007) Simultaneous boninitic and arc-tholeiitic volcanisms in the Izu forearc region
751 during early arc volcanism, based on ODP Leg 125 Site 786. Contrib to Mineral Petrol 153:509–531

752 Hattori KH, Guillot S (2003) Volcanic fronts form as a consequence of serpentinite dehydration in the
753 forearc mantle wedge. Geology 31:525–528

754 Herzig PM, Hannington MD (1995) Polymetallic massive sulfides at the modern seafloor: A review. Ore
755 Geol Rev 10:95–115

756 Herzig P, Hannington M, Arribas Jr A (1998) Sulfur isotopic composition of hydrothermal precipitates from
757 the Lau back-arc: implications for magmatic contributions to seafloor hydrothermal systems. Miner Depos
758 33:226–237

759 Honnorez JA, Jeffrey C, Honnorez-Guerstein BM, Laverne C, Muehlenbachs K, Saltzman E (1985)
760 Stockwork-like sulfide mineralization in young oceanic crust; Deep Sea Drilling Project Hole 504B. Initial
761 Reports Deep Sea Drill Proj 83:263–282

762 Huston DL, Large RR (1989) A chemical model for the concentration of gold in volcanogenic massive
763 sulphide deposits. Ore Geol Rev 4:171–200

764 Huston D, Sie S, Suter G (1995) Selenium and its importance to the study of ore genesis: the theoretical
765 basis and its application to volcanic-hosted massive sulfide deposits using pixeprobe analysis. Nucl
766 Instruments Methods Phys Res Sect B Beam Interact with Mater Atoms 104:476–480

767 Ishikawa Y, Sawaguchi T, Iwaya S, Horiuchi M (1976) Delineation of Prospecting Targets for Kuroko
768 Deposits Based on. Min Geol 26:105–117

769 Ixer RA, Alabaster T, Pearce JA (1984) Ore petrography and geochemistry of massive sulphide deposits
770 within the Semail ophiolite, Oman. Trans Inst Min Metall Sect B Appl Earth Sci 93:114–124

771 Jenner FE, O-Neill HSC, Arculus RJ, Mavrogenes JA (2010) The Magnetite Crisis in the Evolution of Arc-
772 related Magmas and the Initial Concentration of Au, Ag and Cu. J Petrol 51:2445–2464

773 Jenner FE, Arculus RJ, Mavrogenes JA, Dyriw NJ, Nebel O, Hauri EH (2012) Chalcophile element
774 systematics in volcanic glasses from the northwestern Lau Basin. Geochem, Geophys Geosyst 13

775 Ji-Hai Y, Xiu-Chun Z, Chen-Zi F, Ling-Hao Z, Dong-Yang S, Ze-Rong J, Ming-Yue H, Li-Jun K (2012)
776 Quantitative analysis of sulfide minerals by laser ablation-inductively coupled plasma-mass spectrometry
777 using glass reference materials with matrix normalization plus sulfur internal standardization calibration.
778 Chinese J Anal Chem 40:201–207

779 Jowitt SM, Jenkin GR, Coogan LA, Naden J (2012) Quantifying the release of base metals from source
780 rocks for volcanogenic massive sulfide deposits: effects of protolith composition and alteration mineralogy.
781 J Geochem Explor 118:47–59

782 Kamenetsky V, Binns R, Gemmell J, Crawford A, Mernagh T, Maas R, Steele D (2001) Parental basaltic
783 melts and fluids in eastern Manus backarc Basin: implications for hydrothermal mineralisation. Earth Planet
784 Sci Lett 184:685–702

785 Keith M, Haase KM, Klemd R, Krumm S, Strauss H (2016) Systematic variations of trace element and
786 sulfur isotope compositions in pyrite with stratigraphic depth in the Skouriotissa volcanic-hosted massive
787 sulfide deposit, Troodos ophiolite, Cyprus. Chem Geol 423:7–18

788 Keith M, Haase KM, Klemd R, et al (2018) Constraints on the source of Cu in a submarine magmatic-
789 hydrothermal system, Brothers volcano, Kermadec island arc. Contrib to Mineral Petrol 173:40

790 Kritikos A (2016) Compositional systematics of sphalerites from western Bergslagen, Sweden. Uppsala
791 University, Sweden

792 Large RR, Gemmell JB, Paulick H, Huston DL (2001) The alteration box plot: A simple approach to
793 understanding the relationship between alteration mineralogy and lithogeochemistry associated with
794 volcanic-hosted massive sulfide deposits. Econ Geol 96:957–971

795 Lee C-TA, Luffi P, Chin EJ, et al (2012) Copper systematics in arc magmas and implications for crust-
796 mantle differentiation. Science (80-) 336:64–68

797 Maslennikov V, Maslennikova S, Large R, Danyushevsky L (2009) Study of trace element zonation in vent
798 chimneys from the Silurian Yaman-Kasy volcanic-hosted massive sulfide deposit (Southern Urals, Russia)
799 using laser ablation-inductively coupled plasma mass spectrometry (LA-ICPMS). Econ Geol 104:1111–
800 1141

801 Mercier-Langevin P, Hannington MD, Dube B, Becu V (2011) The gold content of volcanogenic massive
802 sulfide deposits. Mineral Deposita 46:509–539

803 Mitchell JG, Peate D, Murton BJ, Pearce JA, Arculus RJ, Van der Laan SR (1992) K-Ar dating of samples
804 from Sites 782 and 786 (Leg 125): the Izu-Bonin forearc region. Proc Ocean Drill Program Sci Results 25:
805 203–210

806 Monecke T, Petersen S, Hannington MD, Grant H, Samson IM (2016) The minor element endowment of
807 modern sea-floor massive sulfide deposits and comparison with deposits hosted in ancient volcanic
808 successions. Rev Econ Geol 18:245–306

809 Moss R, Scott SD, Binns RA (2001) Gold content of eastern Manus Basin volcanic rocks: implications for
810 enrichment in associated hydrothermal precipitates. Econ Geol 96:91–107

811 Müller W, Shelley M, Miller P, Broude S (2009) Initial performance metrics of a new custom-designed ArF
812 excimer LA-ICPMS system coupled to a two-volume laser-ablation cell. J Anal At Spectrom 24:209–214

813 Mungall JE, Brenan JM, Godel B, et al (2015) Transport of metals and sulphur in magmas by flotation of
814 sulphide melt on vapour bubbles. Nat Geosci 8:216–219

815 Murton BJ, Peate DW, Arculus RJ, Pearce JA, Van der Laan S (1992) 12. Trace-element geochemistry of
816 786: the Izu-Bonin forearc region. Proc Ocean Drill Program Sci Results 25:211–235

817 Nesbitt BE, St. Louis RM, Muehlenbachs K (1987) Distribution of gold in altered basalts of DSDP Hole
818 504B. Can J Earth Sci 24:201–209

819 Noll P, Newsom H, Leeman W, Ryan JG (1996) The role of hydrothermal fluids in the production of
820 subduction zone magmas: evidence from siderophile and chalcophile trace elements and boron. Geochim
821 Cosmochim Acta 60:587–611

822 Park J-W, Campbell IH, Kim J, Moon J-W (2015) The role of late sulfide saturation in the formation of a
823 Cu-and Au-rich magma: Insights from the platinum group element geochemistry of Niuatahi-Motutahi
824 lavas, Tonga rear arc. J Petrol 56:59–81

825 Patten CGC, Barnes S-J, Mathez EA, Jenner FE (2013) Partition coefficients of chalcophile elements
826 between sulfide and silicate melts and the early crystallization history of sulfide liquid: LA-ICP-MS analysis
827 of MORB sulfide droplets. Chem Geol 358:170-188

828 Patten CGC, Pitcairn IK, Teagle DA, Harris M (2016a) Mobility of Au and related elements during the
829 hydrothermal alteration of the oceanic crust: implications for the sources of metals in VMS deposits. Mineral
830 Deposita 51:1–22

831 Patten CGC, Pitcairn IK, Teagle DAH, Harris M (2016b) Sulphide mineral evolution and metal mobility
832 during alteration of the oceanic crust: Insights from ODP Hole 1256D. Geochim Cosmochim Acta 193:132–
833 159

834 Patten CGC, Pitcairn IK, Teagle DAH (2017) Hydrothermal mobilisation of Au and other metals in supra-
835 subduction oceanic crust: Insights from the Troodos ophiolite. Ore Geol Rev 86:487–508

836 Pearce JA, van der Laan SR, Arculus RJ, Murt BJ, Ishii T, Peate DW, Park IJ (1992) Boninite and
837 harzburgite from Leg 125 (Bonin-Mariana forearc): A case study of magma genesis during the initial stages
838 of subduction. Proc Ocean Drill Program Sci Results 25:623–659

839 Petersen S, Herzig P, Hannington MD (2000) Third dimension of a presently forming VMS deposit: TAG
840 hydrothermal mound, Mid-Atlantic Ridge, 26 N. Mineral Deposita 35:233–259

841 Piercey SJ (2010) An overview of petrochemistry in the regional exploration for volcanogenic massive
842 sulphide (VMS) deposits. Geochem: Explo, Environ, Anal 10:1-18

843 Piercey SJ (2011) The setting, style, and role of magmatism in the formation of volcanogenic massive
844 sulfide deposits. Miner Depos 46:449–471

845 Piercey SJ, Jenner GA, Wilton DHC, et al (1997) The stratigraphy and geochemistry of the southern Pacquet
846 Harbour Group, Baie Verte Peninsula, Newfoundland; implications for mineral exploration. Curr Res Newf

847 Pilote J-L, Piercey SJ (2018) Petrogenesis of the Rambler Rhyolite Formation: Controls on the Ming VMS
848 Deposit and geodynamic implications for The Taconic Seaway, Newfoundland Appalachians, Canada. Am
849 J Sci 318:640–683oundl Labrador Dep Mines Energy 119:139

850 Pitcairn IK, Warwick PE, Milton JA, Teagle DAH (2006a) Method for ultra-low-level analysis of gold in
851 rocks. Anal Chem 78:1290–1295

852 Pitcairn IK, Teagle DAH, Craw D, Olivo GR, Kerrich R, Brewer TS (2006b) Sources of metals and fluids
853 in orogenic gold deposits: insights from the Otago and Alpine Schists, New Zealand. Econ Geol 101:1525–
854 1546

855 de Ronde C E, Hannington M, Stoffers P, Wright I, Ditchburn R, Reyes A, Baker E, Massoth G, Lupton J,
856 Walker S (2005) Evolution of a submarine magmatic-hydrothermal system: Brothers volcano, southern
857 Kermadec arc, New Zealand. Econ Geol 100:1097–1133

858 Seewald JS, Seyfried Jr WE (1990) The effect of temperature on metal mobility in subseafloor hydrothermal
859 systems: constraints from basalt alteration experiments. Earth Planet Sci Lett 101:388–403

860 Seyfried W, Ding K, Berndt ME, Chen X (1999) Experimental and theoretical controls on the composition
861 of mid-ocean ridge hydrothermal fluids. Rev Econ Geol 8:181–200

862 Shanks III WC (2001) Stable isotopes in seafloor hydrothermal systems: vent fluids, hydrothermal deposits,
863 hydrothermal alteration, and microbial processes. Rev Mineral Geochemistry 43:469–525

864 Sillitoe RH, Hannington MD, Thompson JFH (1996) High sulfidation deposits in the volcanogenic massive
865 sulfide environment. Econ Geol 91:204–212

866 Skulski T, Castonguay S, McNicoll V, et al (2010) Tectonostratigraphy of the Baie Verte oceanic tract and
867 its ophiolite cover sequence on the Baie Verte Peninsula. Newfoundl Labrador Dep Nat Resour Geol Surv
868 Rep 1:315–337

869 Stakes DS, Taylor HP (2003) Oxygen isotope and chemical studies on the origin of large plagiogranite
870 bodies in northern Oman, and their relationship to the overlying massive sulphide deposits. Geol Soc
871 London, Spec Publ 218:315–351

872 Stern RA, Syme EC, Bailes AH, Lucas SB (1995) Paleoproterozoic (1.90–1.86 Ga) arc volcanism in the
873 Flin Flon Belt, Trans-Hudson Orogen, Canada. Contrib to Mineral Petrol 119:117–141

874 Sun W, Arculus RJ, Kamenetsky VS, Binns RA (2004) Release of gold-bearing fluids in convergent margin
875 magmas prompted by magnetite crystallization. Nature 431:975–978

876 Sun W, Huang R-f, Li H, Hu Y-b, Zhang C-c, Sun S-j, Zhang L-p, Ding X, Li C-y, Zartman RE (2015)
877 Porphyry deposits and oxidized magmas. Ore Geol Rev 65:97–131

878 Syme EC, Lucas SB, Bailes AH, Stern RA (2000) Contrasting arc and MORB-like assemblages in the
879 Paleoproterozoic Flin Flon Belt, Manitoba, and the role of intra-arc extension in localizing volcanic-hosted
880 massive sulphide deposits. Can J Earth Sci 36:1767–1788

881 Teagle D, Alt J, Umino S, Miyashita S, Banerjee N, Wilson D, the Expedition 309/312 Scientists (2006)
882 Superfast spreading rate crust 2 and 3. Proceedings of Integrated Ocean Drilling Program. 309 312, 50

883 Terashima S, Yuasa M, Nohara M (1994) Gold content of submarine volcanic rocks from the Izu-Ogasawara
884 (Bonin) arc. Resour Geol 44:241–247

885 Timm C, de Ronde CE, Leybourne MI, Layton-Matthews D, Graham IJ (2012) Sources of chalcophile and
886 siderophile elements in Kermadec arc lavas. Econ Geol 107:1527–1538

887 Webber AP, Roberts S, Taylor RN, Pitcairn IK (2013) Golden plumes: Substantial gold enrichment of
888 oceanic crust during ridge-plume interaction. Geology 41:87–90

889 Wilson SA, Ridley WI, Koenig AE (2002) Development of sulfide calibration standards for the laser
890 ablation inductively-coupled plasma mass spectrometry technique. J Anal At Spectrom 17:406–409

891 Wohlgemuth-Ueberwasser CC, Viljoen F, Petersen S, Vorster C (2015) Distribution and solubility limits of
892 trace elements in hydrothermal black smoker sulfides: An in-situ LA-ICP-MS study. Geochim Cosmochim
893 Acta 159:16–41

894 Yang K, Scott SD (2002) Magmatic degassing of volatiles and ore metals into a hydrothermal system on
895 the modern sea floor of the eastern Manus back-arc basin, western Pacific. Econ Geol 97:1079–1100

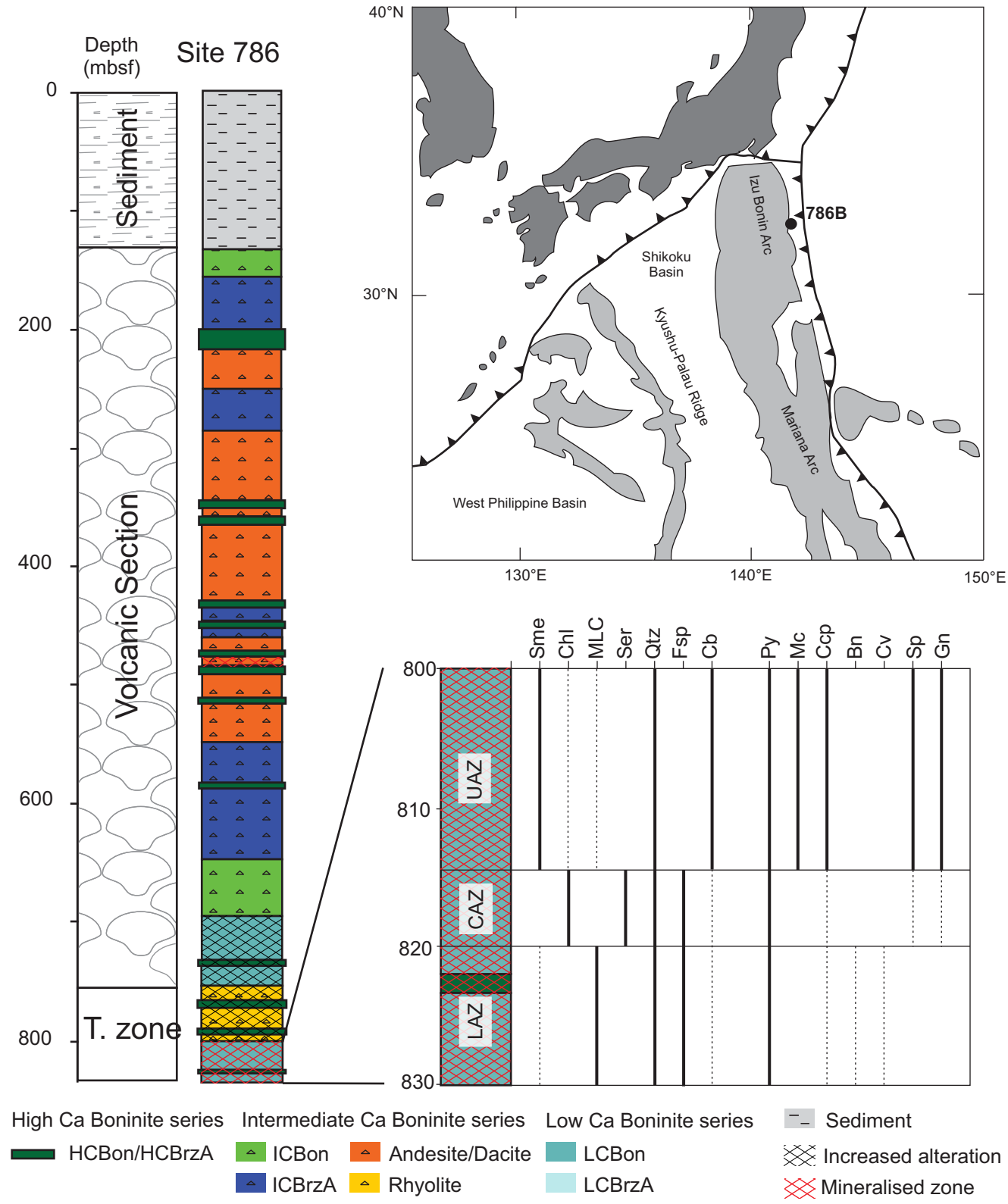
Depth (mbsf)
Site 786
0
200
400
600
800
Sediment
Volcanic Section
T. zone
40°N
30°N
130°E
140°E
150°E
786B
Izu Bonin Arc
Shikoku Basin
Kyushu-Palau Ridge
Mariana Arc
West Philippine Basin
Sme
Chl
MLC
Ser
Qtz
Fsp
Cb
Py
Mc
Ccp
Bn
Cv
Sp
Gn
800
810
820
830
UAZ
CAZ
LAZ
High Ca Boninite series
HCBon/HCBrzA
Intermediate Ca Boninite series
ICBon
ICBrzA
Andesite/Dacite
Rhyolite
Low Ca Boninite series
LCBon
LCBrzA
Sediment
Increased alteration
Mineralised zone

Fig. 1

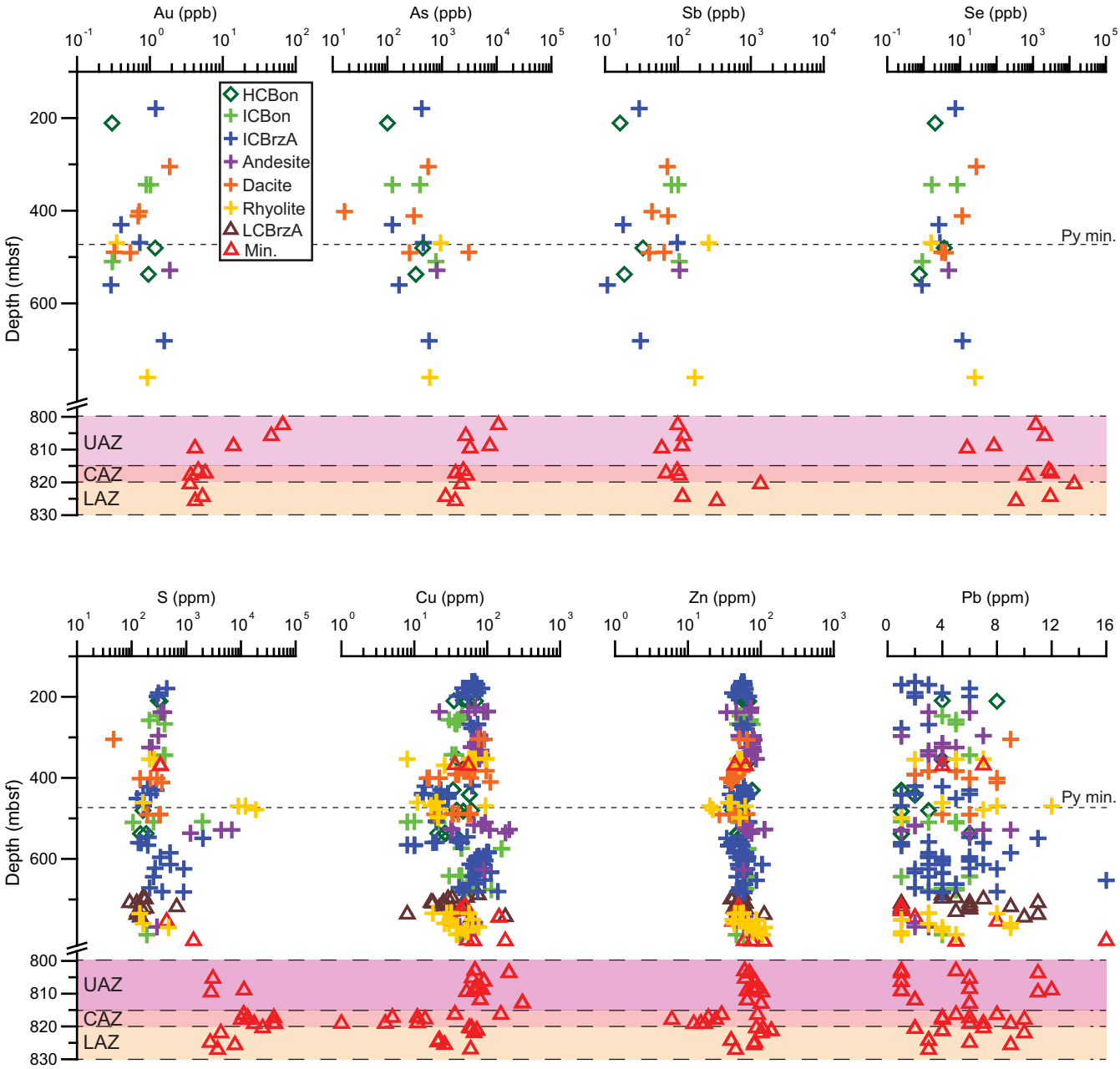
Au (ppb)
As (ppb)
Sb (ppb)
Se (ppb)
HCBon
ICBon
ICBrzA
Andesite
Dacite
Rhyolite
LCBrzA
Min.
Depth (mbsf)
Py min.
UAZ
CAZ
LAZ

S (ppm)
Cu (ppm)
Zn (ppm)
Pb (ppm)
Depth (mbsf)
Py min.
UAZ
CAZ
LAZ

Figure 2.

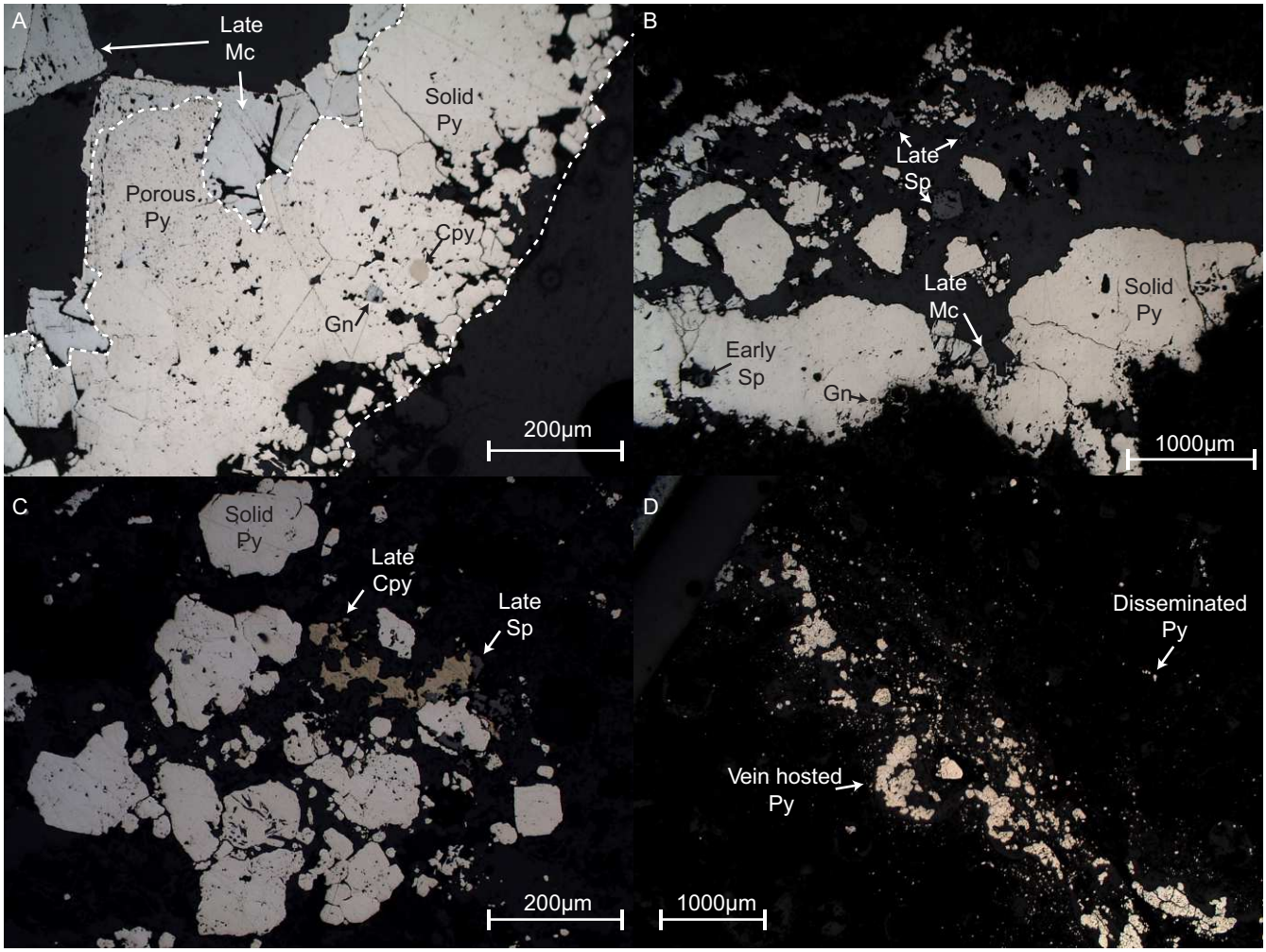
A
Late
Mc
Solid
Py
Porous
Py
Cpy
Gn
200µm
B
Late
Sp
Late
Mc
Solid
Py
Early
Sp
Gn
1000µm
C
Solid
Py
Late
Cpy
Late
Sp
200µm
D
Disseminated
Py
Vein hosted
Py
1000µm

Figure 3.

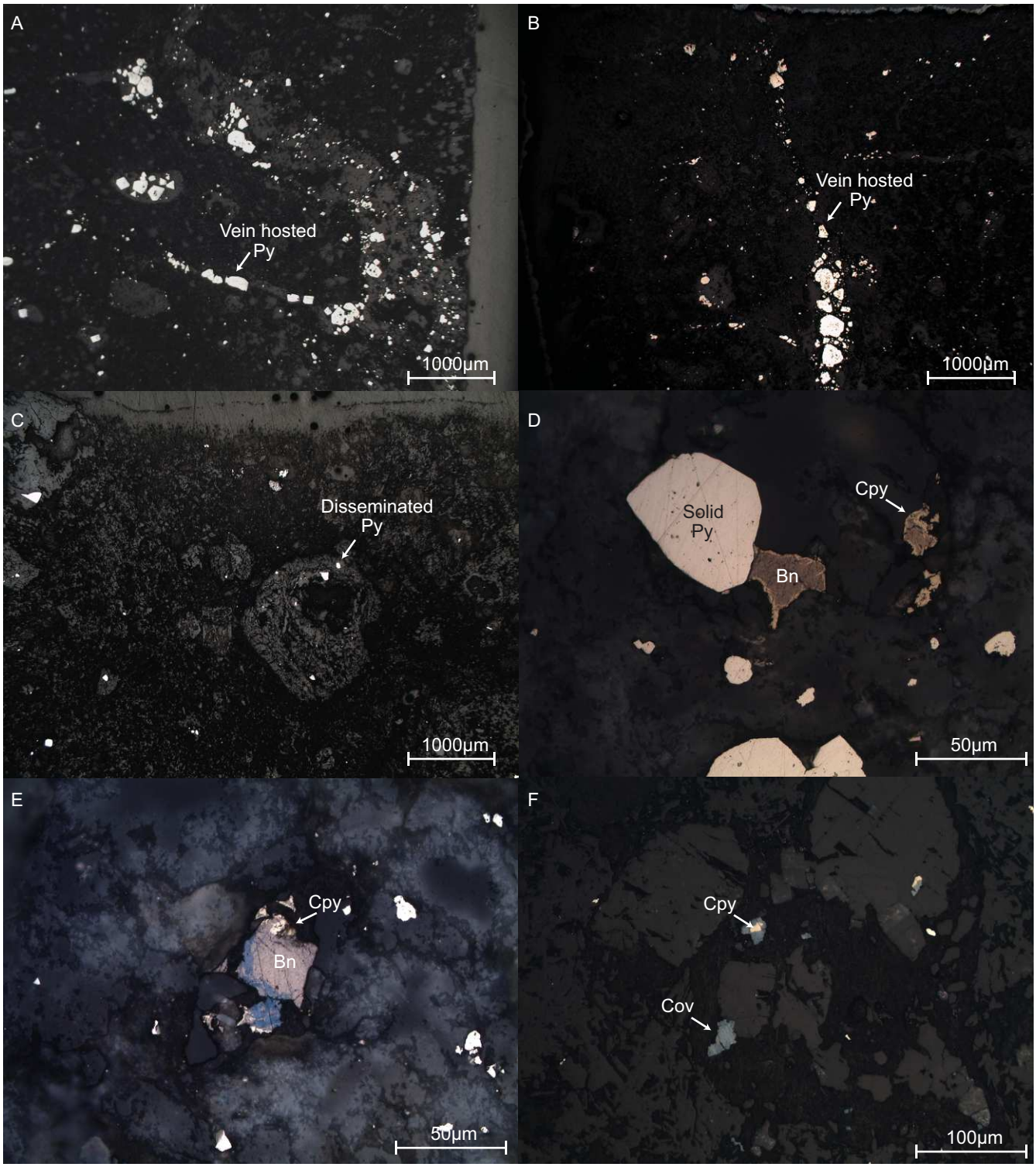
A
Vein hosted
Py
1000µm
B
Vein hosted
Py
1000µm
C
Disseminated
Py
1000µm
D
Solid
Py
Cpy
Bn
50µm
E
Cpy
Bn
50µm
F
Cpy
Cov
100µm

Figure 4.

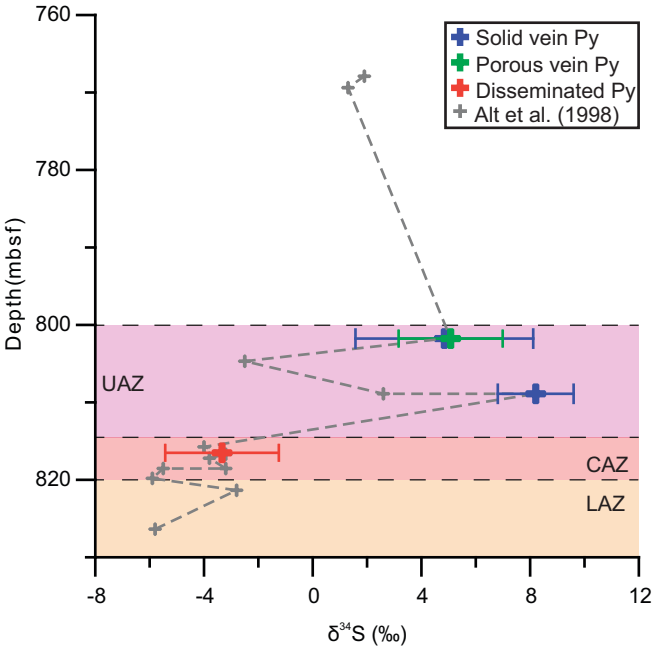
760
780
800
820
Depth (mbsf)
Solid vein Py
Porous vein Py
Disseminated Py
Alt et al. (1998)
UAZ
CAZ
LAZ
-8
-4
0
4
8
12
δ34S (‰)

Fig. 5

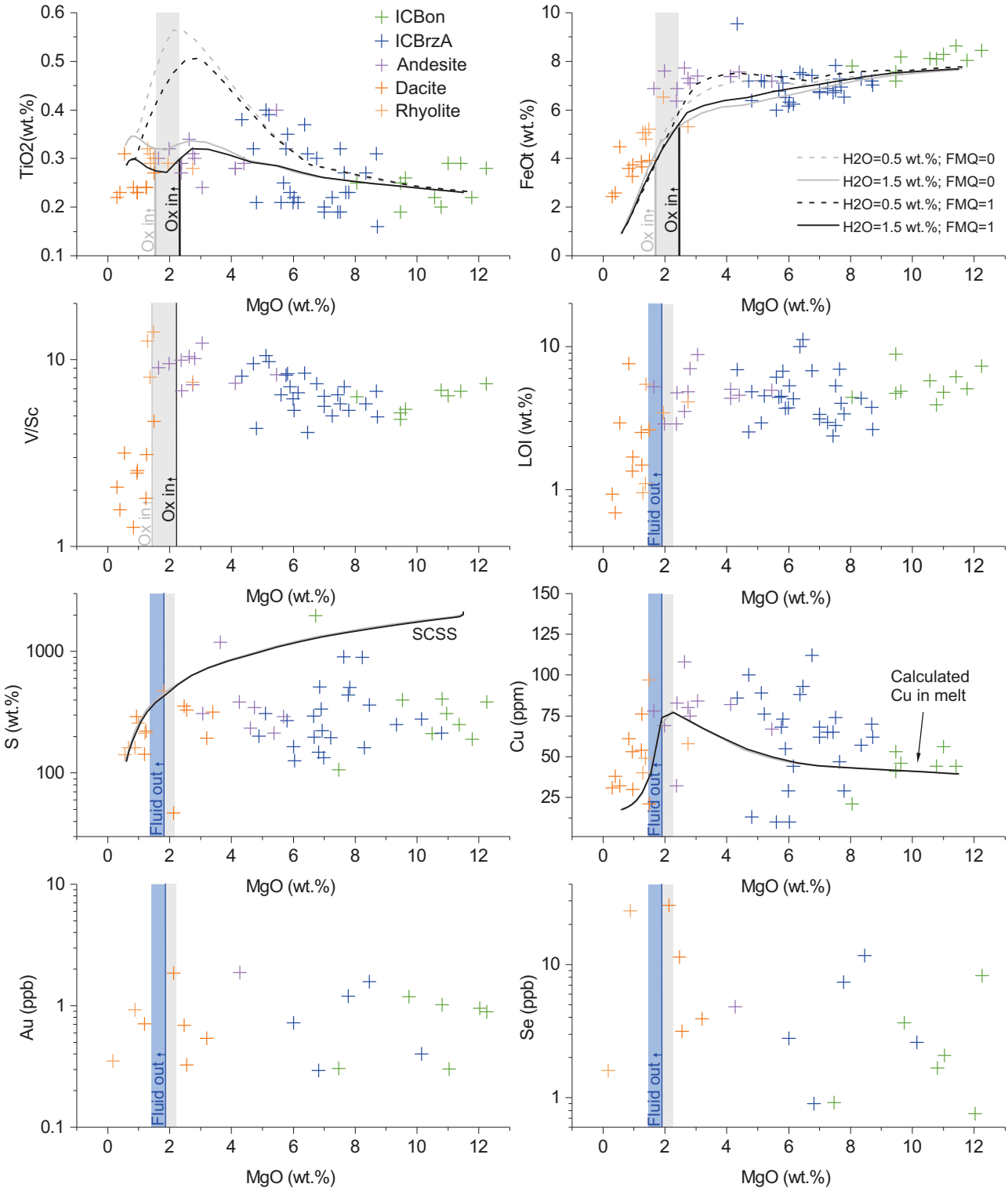
ICBon
ICBrzA
Andesite
Dacite
Rhyolite
TiO2(wt.%)
FeOt (wt.%)
H2O=0.5 wt.%; FMQ=0
H2O=1.5 wt.%; FMQ=0
H2O=0.5 wt.%; FMQ=1
H2O=1.5 wt.%; FMQ=1
Ox in
MgO (wt.%)
V/Sc
LOI (wt.%)
Fluid out
S (wt.%)
SCSS
Cu (ppm)
Calculated
Cu in melt
Au (ppb)
Se (ppb)

Figure 6.

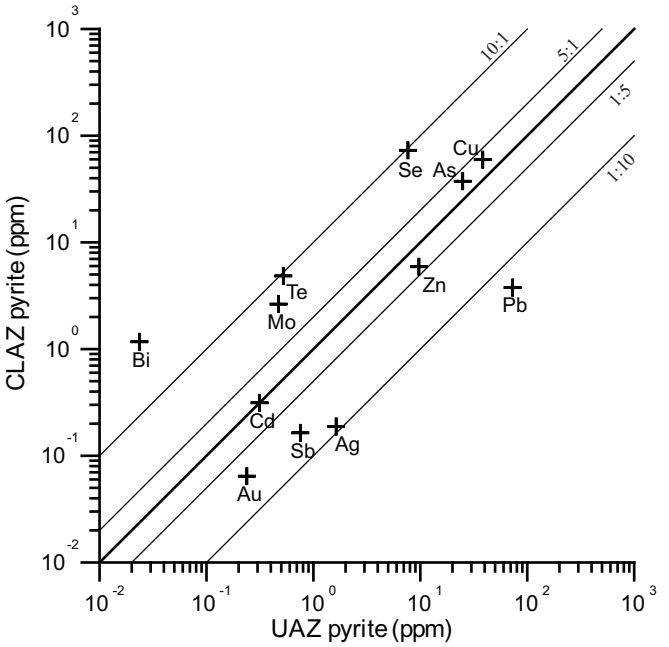
CLAZ pyrite (ppm)
UAZ pyrite (ppm)
10:1
5:1
1:5
1:10
Se
As
Cu
Te
Mo
Zn
Pb
Bi
Cd
Sb
Ag
Au

Figure 7.

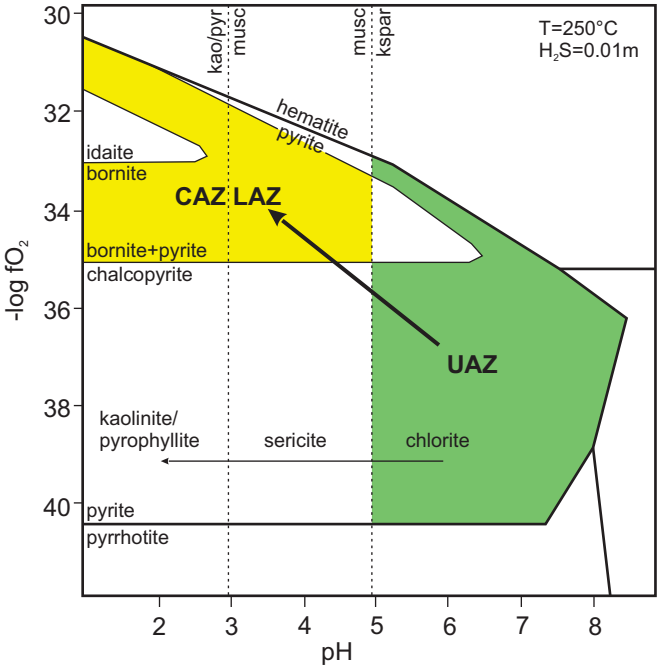
30
32
34
36
38
40
-log fO2
2
3
4
5
6
7
8
pH
kao/pyr
musc
musc
kspar
T=250°C
H2S=0.01m
hematite
pyrite
idaite
bornite
CAZ
LAZ
bornite+pyrite
chalcopyrite
UAZ
kaolinite/
pyrophyllite
sericite
chlorite
pyrite
pyrrhotite

Figure 8.

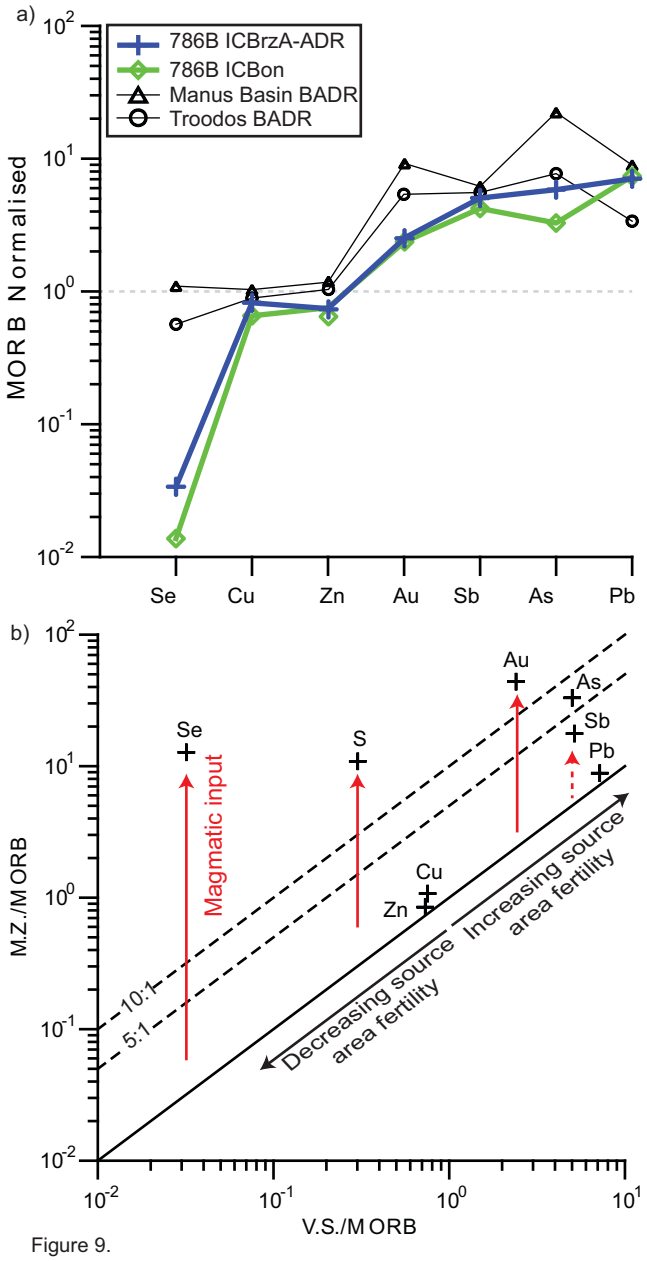
a)
786B ICBrzA-ADR
786B ICBon
Manus Basin BADR
Troodos BADR
MORB Normalised
Se
Cu
Zn
Au
Sb
As
Pb
b)
M.Z./MORB
V.S./MORB
Magmatic input
10:1
5:1
Increasing source area fertility
Decreasing source area fertility

Figure 9.

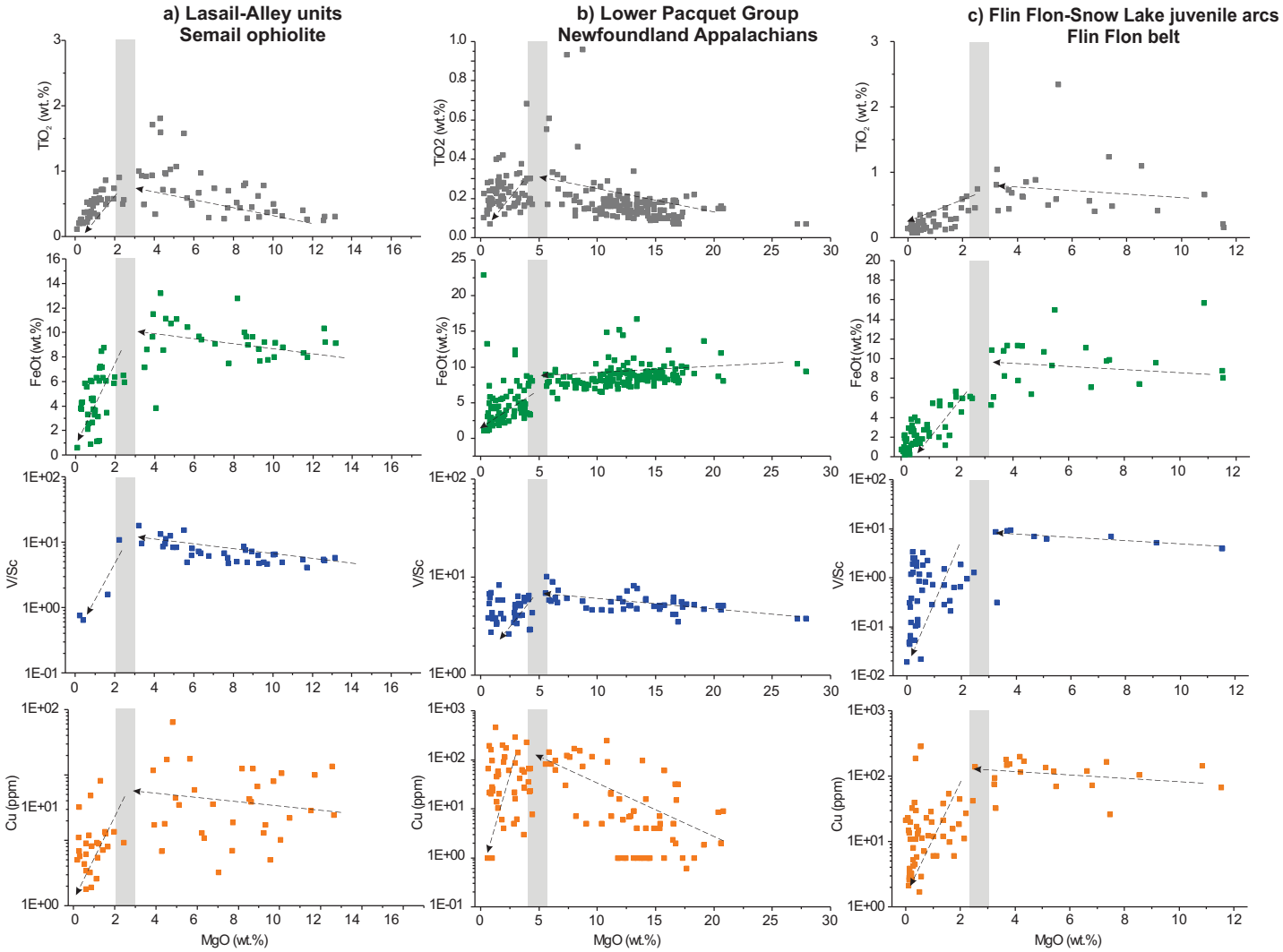
a) Lasail-Alley units
Semail ophiolite
b) Lower Pacquet Group
Newfoundland Appalachians
c) Flin Flon-Snow Lake juvenile arcs
Flin Flon belt
TiO2 (wt.%)
FeOt (wt.%)
V/Sc
Cu (ppm)
MgO (wt.%)

Figure. 10

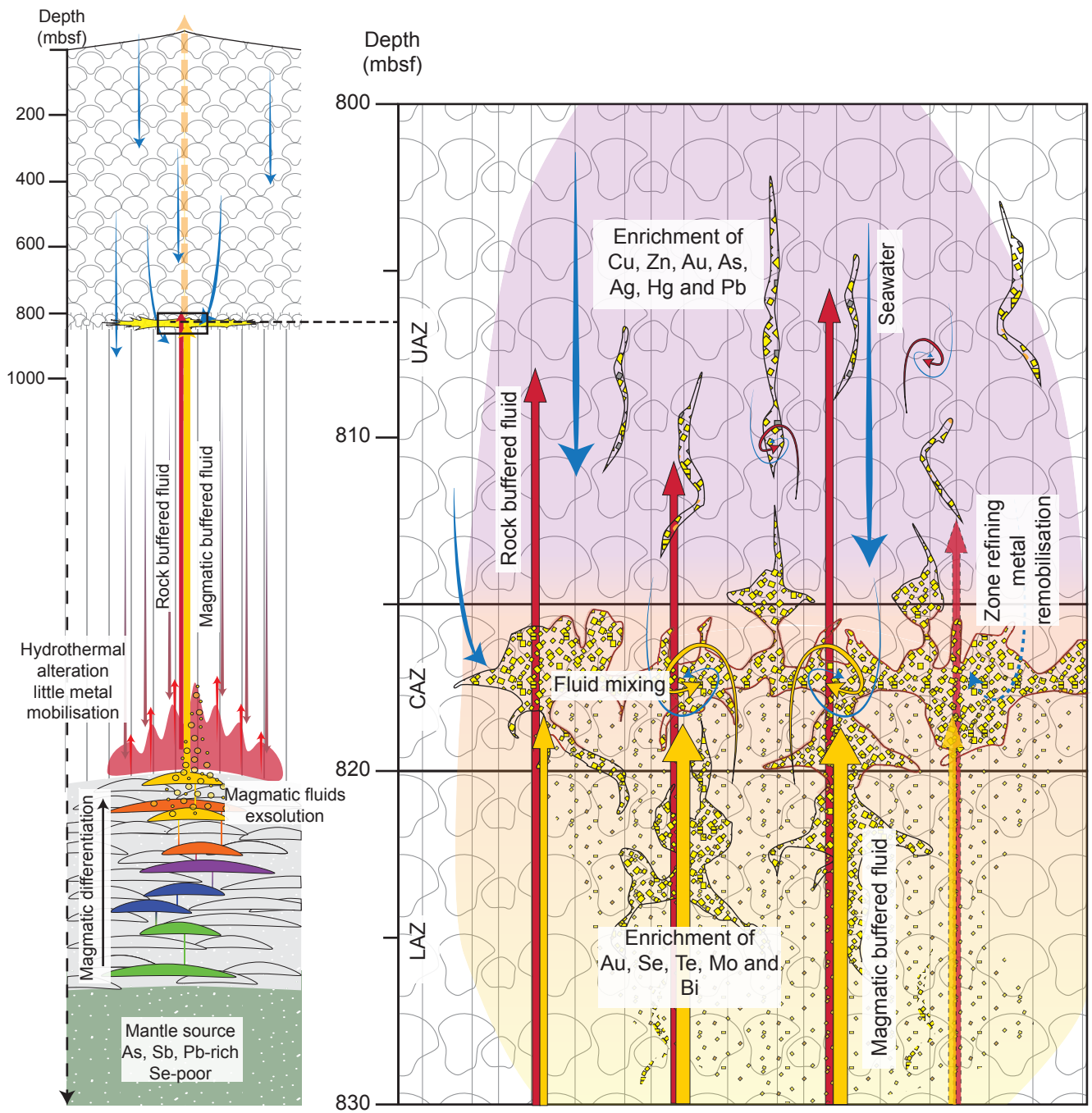
Depth
(mbsf)
200
400
600
800
1000
Rock buffered fluid
Magmatic buffered fluid
Hydrothermal
alteration
little metal
mobilisation
Magmatic fluids
exsolution
Magmatic differentiation
Mantle source
As, Sb, Pb-rich
Se-poor
Depth
(mbsf)
800
810
820
830
UAZ
CAZ
LAZ
Enrichment of
Cu, Zn, Au, As,
Ag, Hg and Pb
Seawater
Rock buffered fluid
Zone refining
metal
remobilisation
Fluid mixing
Enrichment of
Au, Se, Te, Mo and
Bi
Magmatic buffered fluid

Figure 14.

Table 1. Whole rock data of Hole 786B lithologies and mineralised zone

			Au (ppb)	As (ppb)	Sb (ppb)	Se (ppb)	S (ppm)	Cu (ppm)	Zn (ppm)	Pb (ppm)
Volcanic section least altered samples										
High Ca Boninite series	HCBon	average (n=3)	0.81	292	22.5	2.16	2.26E+02	45.7	60.3	2.67
		σ	0.46	175	9.2	1.45	8.67E+01	14.1	9.9	2.16
		median	0.95	332	18.4	2.07	1.85E+02	47.0	61.0	2.00
Inter Ca Boninite series	ICBon	average (n=3)	0.74	429	95.6	3.62	4.70E+02	48.9	63.2	4.17
		σ	0.38	325	12.4	4.05	5.74E+02	31.8	7.5	1.53
		median	0.89	394	101.0	1.67	3.09E+02	44.0	62.0	5.00
	ICBrzA	average (n=5)	0.84	349	37.2	5.06	3.97E+02	56.0	56.5	3.83
		σ	0.54	197	34.9	4.40	4.11E+02	28.6	11.0	2.63
		median	0.73	426	29.4	2.78	2.69E+02	62.0	58.0	3.00
	Andesite	average (n=1)	1.87	808	105	4.82	1.57E+03	77.5	71.6	3.60
		σ					2.38E+03	31.6	15.2	2.10
		median					3.45E+02	78.0	72.0	3.00
	Dacite	average (n=5)	0.83	845	58.6	11.6	2.38E+02	49.3	47.6	5.21
		σ	0.60	1270	15.5	11.5	1.07E+02	24.4	9.4	2.22
		median	0.69	306	64.6	7.7	2.57E+02	49.0	48.0	5.50
	Rhyolite	average (n=2)	0.64	768	218	13.4	4.58E+03	42.8	60.7	4.33
		σ	0.41	243	66.2	16.7	6.98E+03	23.9	22.5	3.16
		median	0.64	768	218	13.4	2.58E+02	35.0	54.0	3.50
Low Ca Boninite series	LCBon /BrzA	average (n=10)	15.8	3640	248	2677	1.20E+04	75.2	66.5	5.04
		σ	22.1	3040	397	3991	1.32E+04	65.1	31.8	3.50
		median	4.93	2580	109	1652	8.94E+03	65.0	65.0	5.00
Mineralised zone (796-828 mbsf)										
Upper alteration zone	799-815 mbsf	average (n=4)	32.7	6050	99	851	5.76E+03	106	75.3	4.2
		σ	28.8	3780	27	997	4.87E+03	76.4	17.5	3.7
		median	30.1	5360	107	640	3.06E+03	75.0	70.0	2.0
Central alteration zone	815-820 mbsf	average (n=4)	4.38	2330	407	5010	2.23E+04	37.7	43.0	5.8
		σ	1.04	441	633	5760	1.32E+04	45.3	41.4	2.6
		median	4.11	2360	101	2940	1.55E+04	14.0	21.5	6.0
Lower alteration zone	820-828 mbsf	average (n=2)	4.72	1450	229	1660	4.63E+03	45.0	83.4	5.3
		σ	0.77	413	160	1860	2.19E+03	24.2	41.3	2.8
		median	4.72	1450	229	1660	4.01E+03	42.5	82.0	4.0

No HCBrzA have been analysed. Low Ca boninite series corresponds to the mineralised zone between 796-828 mbsf. n= number of samples analysed for Au, As, Sb and Se. S, Cu, Zn and Pb data are compiled from Arculus et al. (1992), Alt et al. (1998) and Haraguchi and Teruaki (2014).

Table 2. Trace metal content of sulphides from the upper, central and lower alteration zones

		Cu (ppm)	Zn (ppm)	As (ppm)	Se (ppm)	Mo (ppm)	Ag (ppm)	Cd (ppm)	Sb (ppm)	Te (ppm)	Au (ppm)	Pb (ppm)	Bi (ppm)
Upper alteration zone													
Solid pyrite	average	88	15	110	19	2.6	5.2	0.73	4.9	3.6	1.3	170	0.086
	σ	150	13	210	71	5	10	2.8	15	15	2.8	320	0.27
	median	**36**	**9.3**	**18**	**7.7**	**0.47**	**1.1**	**0.31**	**0.39**	**0.52**	**0.16**	**52**	**0.024**
Porous pyrite	average	31	9.0	66	b.d.l.	0.86	2	1.4	1.3	1.2	0.46	110	0.15
	σ	35	13	98		1.5	3.3	3.9	2.5	1.7	0.61	120	0.27
	median	**19**	**4.1**	**22**		**0.47**	**0.98**	**0.31**	**0.42**	**0.52**	**0.25**	**78**	**0.038**
Marcasite	average	57	13	19	b.d.l.	0.52	1.6	0.63	0.17	b.d.l.	0.7	48	b.d.l.
	σ	81	12	4.3		0.12	1.4	0.73	0.2		0.86	130	
	median	**43**	**8.7**	**18**		**0.47**	**1.4**	**0.31**	**0.078**		**0.37**	**7.6**	
Sphalerite	average	2.1E+04	5.7E+05	18	8.2	1.2	4.5	1900	0.67	0.57	0.062	640	0.031
	σ	2.2E+04	1.0E+05	24	1.8	2.5	4.6	1300	1.4	0.16	0.054	2100	0.013
	median	**1.3E+04**	**6.0E+05**	**11**	**7.7**	**0.47**	**2.1**	**1600**	**0.19**	**0.52**	**0.026**	**52**	**0.024**
Chalcopyrite	average	2.1E+05	380	22	8.2	2	2.8	26	0.78	0.54	0.25	220	0.49
	σ	3.6E+04	320	10	0.57	0.27	1.4	18	0.19	0.019	0.03	130	0.012
	median	**2.1E+05**	**380**	**22**	**8.2**	**2**	**2.8**	**26**	**0.78**	**0.54**	**0.25**	**220**	**0.49**
Galena	average	33	5.9	33	110	2.7	150	94	120	0.82	0.032	8.5E+05	3.3
	σ	37	2.9	10	96	2.2	84	4.2	89	0.25	0.015	2.4E+04	2.3
	median	**13**	**3.9**	**29**	**50**	**1.9**	**130**	**92**	**85**	**0.81**	**0.022**	**8.7E+05**	**2**
Central alteration zone													
Disseminated pyrite	average	150	31	70	81	5.1	0.29	1.6	0.48	11	0.11	10	3.2
	σ	160	41	120	58	3.4	0.17	3.3	0.50	11	0.11	10	1.9
	median	**100**	**10**	**33**	**80**	**3.8**	**0.19**	**0.3**	**0.38**	**8.4**	**0.07**	**5.2**	**3.0**
Vein pyrite	average	270	12	120	120	6.0	0.23	b.d.l.	0.13	7.2	0.06	58	0.8
	σ	370	16	170	120	5.3	0.07		0.11	7.8	0.04	190	1.2
	median	**110**	**3.9**	**59**	**100**	**3.7**	**0.19**		**0.08**	**4.0**	**0.06**	**1.4**	**0.6**
Lower alteration zone													
Disseminated pyrite	average	110	5.3	95	69	1.1	0.35	0.4	0.74	5.4	0.09	50	3.0
	σ	230	1.5	110	97	0.8	0.43	0.2	0.80	7.4	0.06	41	4.2
	median	**25**	**4.7**	**51**	**12**	**0.8**	**0.19**	**0.3**	**0.30**	**1.9**	**0.07**	**36**	**1.3**
Bornite	average	5.6E+05	39	57	290	3.3	14.00	3.2	1.80	0.58	0.12	65	50
	σ	2.4E+04	71	25	140	5.6	8.20	1.4	3.50	0.11	0.15	78	8.4
	median	**5.5E+05**	**3.9**	**72**	**320**	**0.5**	**8.90**	**2.8**	**0.09**	**0.52**	**0.03**	**39**	**51**

b.d.l.=below detection limit